Topological and Multipolar Magnets and Spintronics

Satoru Nakatsuji

Dept. of Physics, University of Tokyo
Institute for Solid State Physics (ISSP), University of Tokyo
Institute of Quantum Matters (IQM), Johns Hopkins University

New material platforms: Blending electronic band topology with multipoles

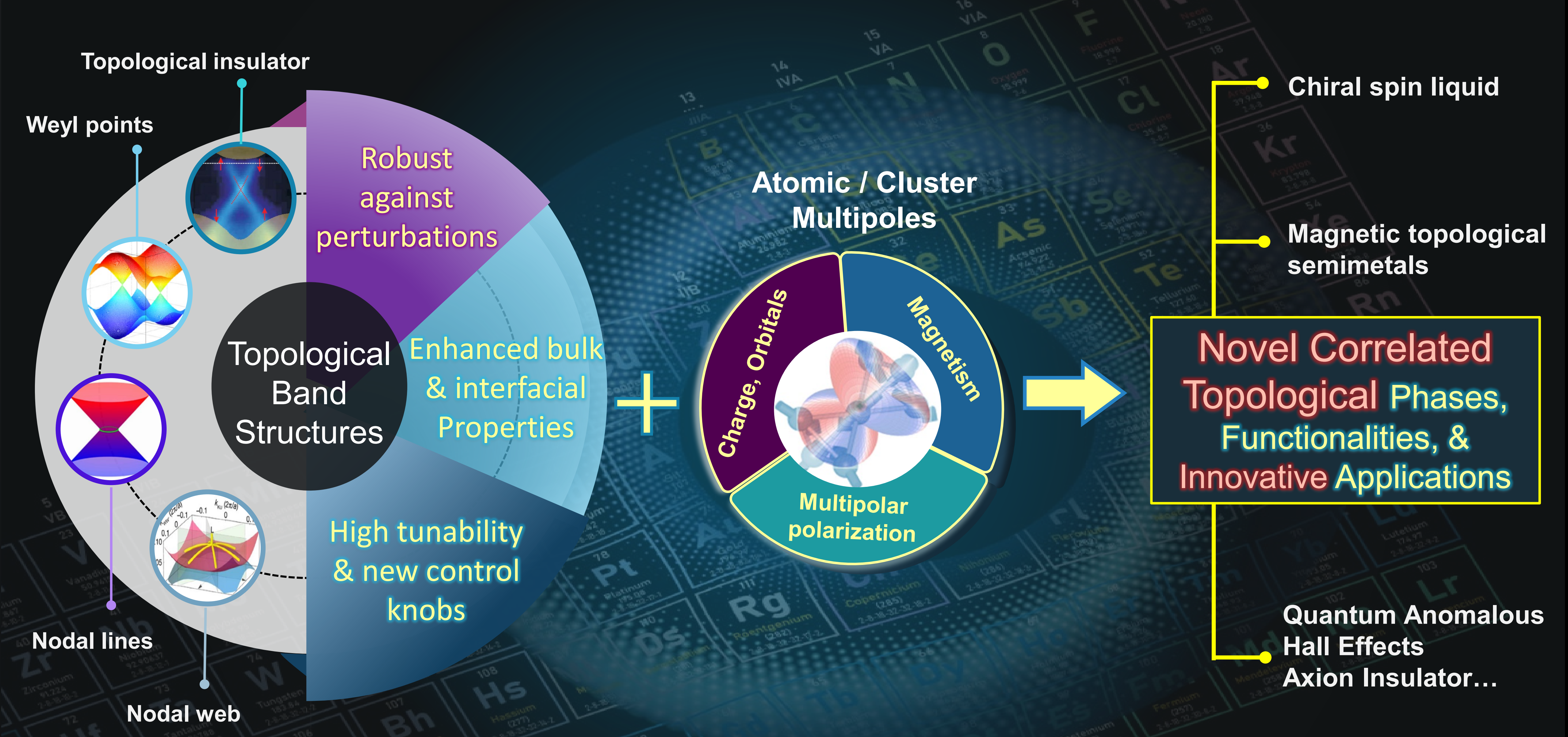

Plan

- Multipole Physics on Correlated Electron Systems
- Topological States in Magnetic Systems
- Physics of Antiferromagnetic Weyl Semimetals
- Physics of Multipolar Kondo Lattice Systems

Plan

- Multipole Physics on Correlated Electron Systems
- Topological States in Magnetic Systems
- Physics of Antiferromagnetic Weyl Semimetals
- Physics of Multipolar Kondo Lattice Systems

Lecture 3

- Magnetic Weyl Semimetals
- Weyl Semimetallic State in Antiferromagnet Mn_3X
- Manipulation
  - Electrical Current Control through Spin Orbit Torque
- Quantum Coherent Transport
  - Tunneling Magnetoresistances

Weyl Semimetal State

X. Wan, A. M. Turner, A. Vishwanath, and S. Y. Savrasov, 2011

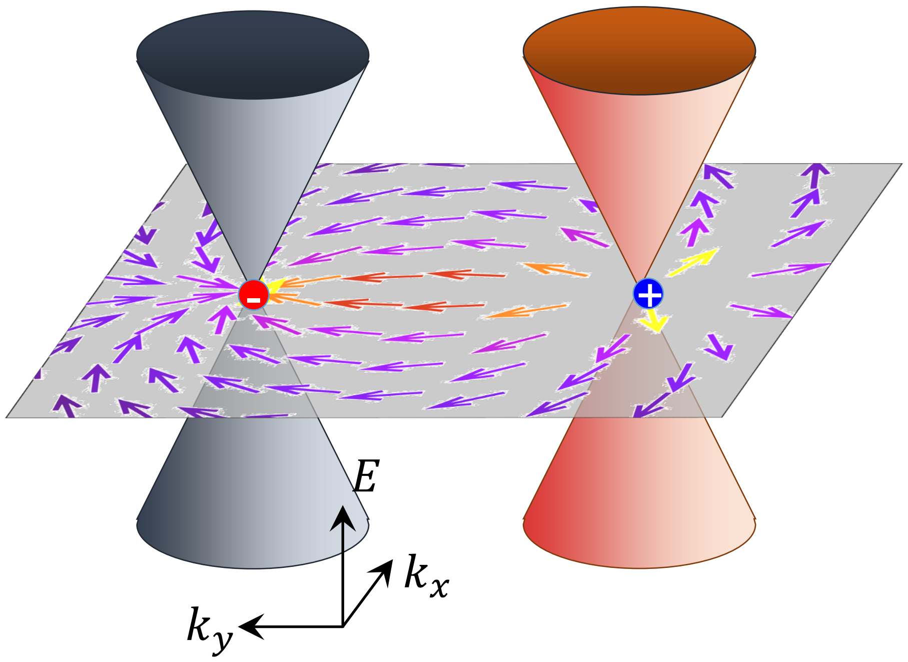

Topological Metal with broken spatial inversion/ time reversal symmetry.

Pair of Linearly dispersive excitation Similar to Graphene, but in 3D.

Weyl Eq. $\mathcal{H} = \sum_{i=1}^{3} \mathbf{v}_i \cdot \mathbf{k} \ \sigma_i$

Robust against Symm. Breaking perturbation

Crossing points:
Magnetic Monopoles

Source and sink of Berry curvature/ Fictitious Field

- **Layered Quantum Hall Effect**
- **Chiral Anomaly**

Chern number for a single Weyl point

$\gamma\vec{p}\vec{\sigma}|\psi\rangle = E|\psi\rangle$ Weyl Equation

→ Same as magnetic monopole in real space! $H = \frac{1}{2}\vec{B}\vec{\sigma}$

- Eigen energies: $E = \pm|\vec{p}|$
- Eigen states: $|\psi_+\rangle = \begin{pmatrix} e^{-i\phi}\cos\theta/2 \\ \sin\theta/2 \end{pmatrix}$ $|\psi_-\rangle = \begin{pmatrix} -e^{-i\phi}\sin\theta/2 \\ \cos\theta/2 \end{pmatrix}$
- Berry curvature: $\Omega_{\boldsymbol{k}} = \mp\gamma\frac{\vec{p}}{2p^3}$

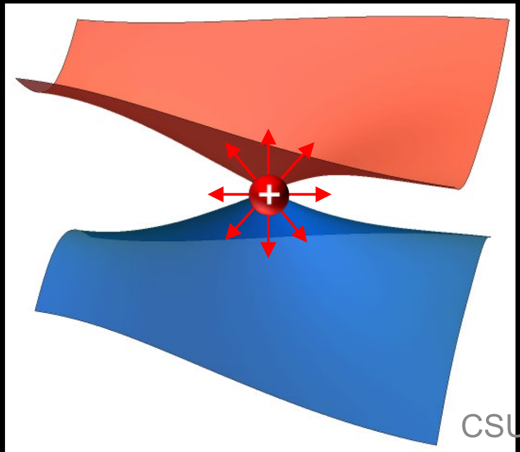

e.g. for $\gamma = -1$,

- Chern number $C = \frac{\int \Omega_{\boldsymbol{k}} d\boldsymbol{S}}{2\pi} = +1$
- monopole charge $Q = \frac{C}{2} = +1/2$

A pair of Weyl points

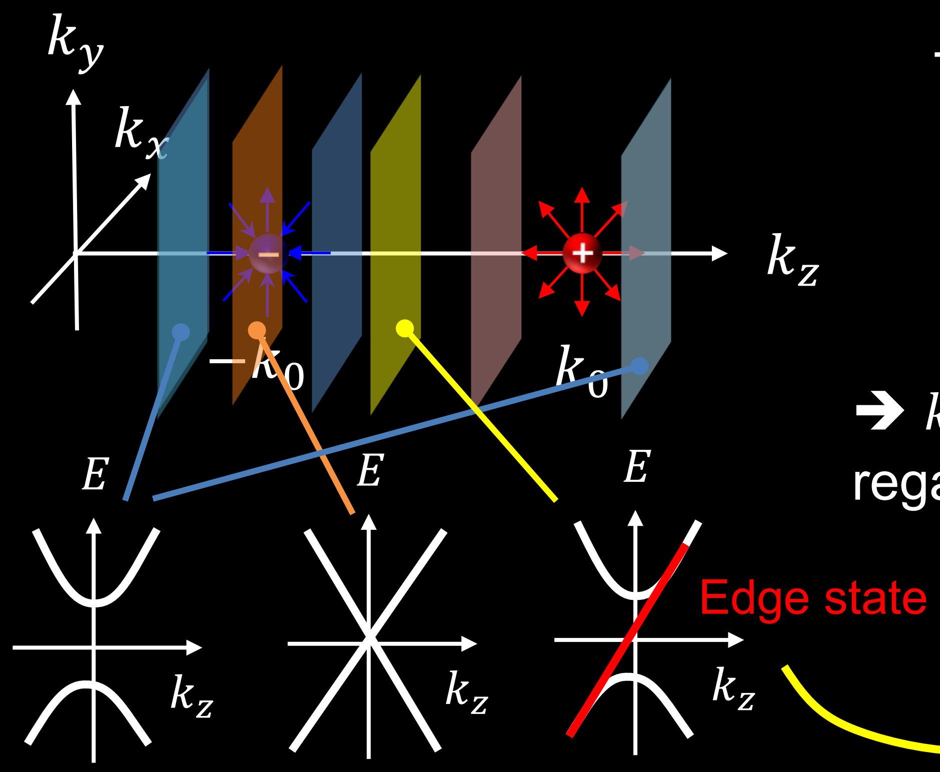

Insulator

Weyl $(k = \pm k_0)$

Quantum Hall $(-k_0 < k_z < k_0)$

To satisfy the Gauss's theorem,

$$C = \begin{cases} 1 & (-k_0 < k_z < k_0) \\ 0 & (k_z < -k_0, k_0 < k_z) \end{cases}$$

➔ k_x- k_y plane at $-k_0 < k_z < k_0$ can be regarded as the quantum Hall system.

Surface state (Fermi arc)

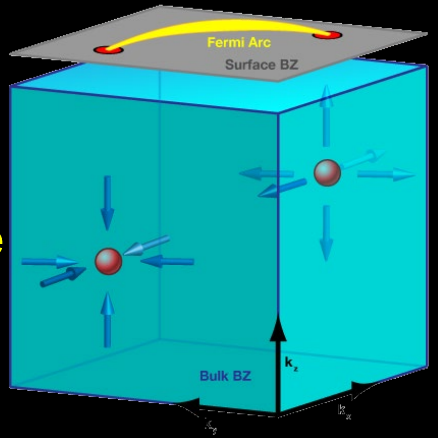

□ Hall conductivity

$$\sigma_{xy} = -\frac{e^2}{(2\pi)^2 \hbar} \int_{-k_0}^{k_0} 1 \, dk_z = -\frac{e^2}{(2\pi)^2 \hbar} (2k_0)$$

Nielsen-Ninomiya theorem 1983

- Bloch Bands in 3D Brillouin Zone

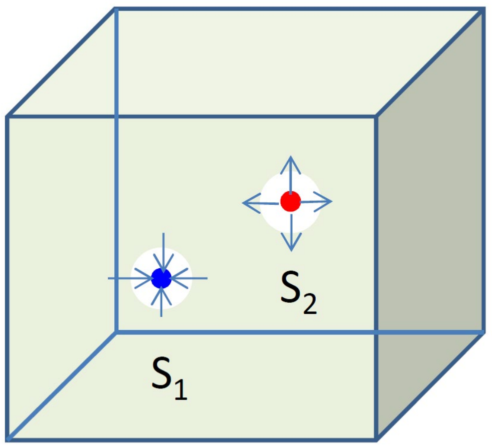

Weyl nodes appears in pair with opposite chiralities

- Sign of a monopole charge depends on band-*n* and chiralities

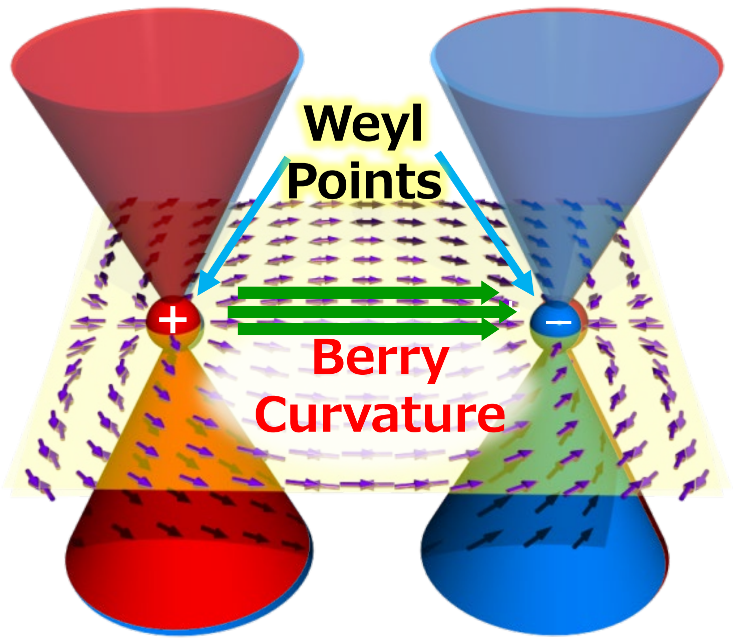

Weyl Nodes and Symmetry

Dirac

$\mathcal{T}$ ($k \rightarrow -k$, $\sigma_i \rightarrow -\sigma_i$)

$\mathcal{I}$ ($k \rightarrow -k$)

$E_{n,\sigma}(\mathrm{k}) = E_{n,-\sigma}(\mathrm{k})$

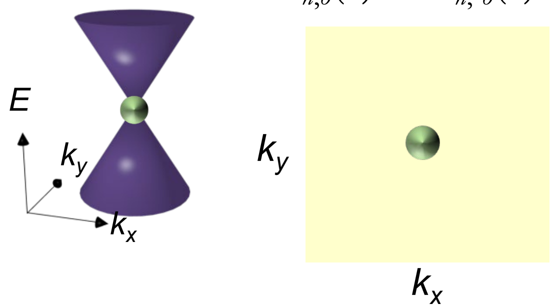

$\mathcal{I}$-breaking

$\mathcal{T}$-breaking

Weyl

$\mathcal{T}$ ($k \rightarrow -k$, $\sigma_i \rightarrow -\sigma_i$)

$E_{n,\sigma}(\mathrm{k}) = E_{n,-\sigma}(\mathrm{-k})$

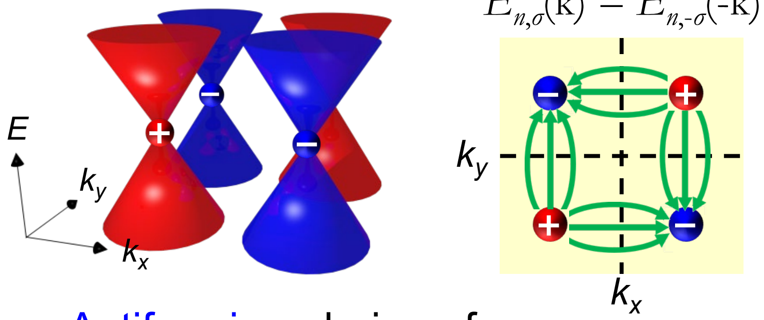

Antiferroic ordering of Weyl points/Berry curvature

$\mathcal{I}$ ($k \rightarrow -k$)

$E_{n,\sigma}(\mathrm{k}) = E_{n,\sigma}(\mathrm{-k})$

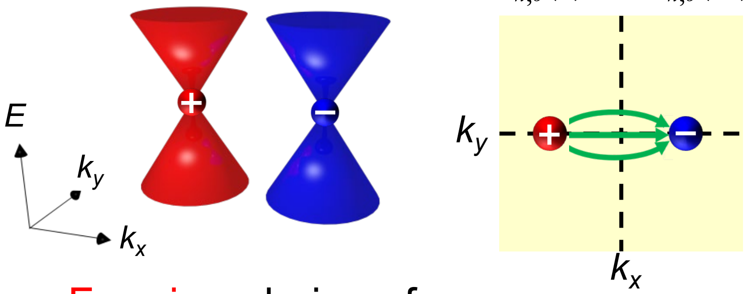

Ferroic ordering of Weyl points/Berry curvature

➡ Zero-field AHE, ANE, & MOKE

$\mathcal{T}$-breaking Weyl semimetal = Weyl magnet has non-zero Berry curvature

showing large zero-field electrical, thermal, & optical responses

I-breaking Weyl semimetal: TaAs

ARPES (Angle resolved photoemission spectroscopy)

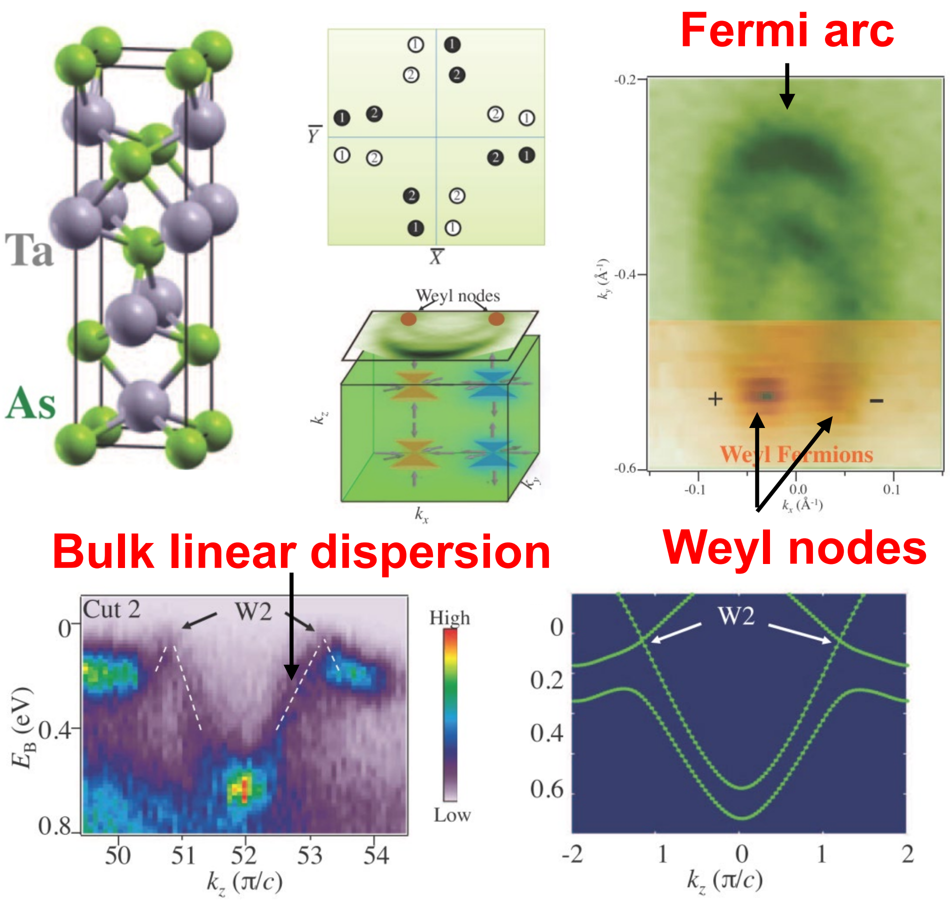

Xu *et al.*, Science **349**, 613 (2015); Lv *et al.*, PRX **5**, 031013 (2015).

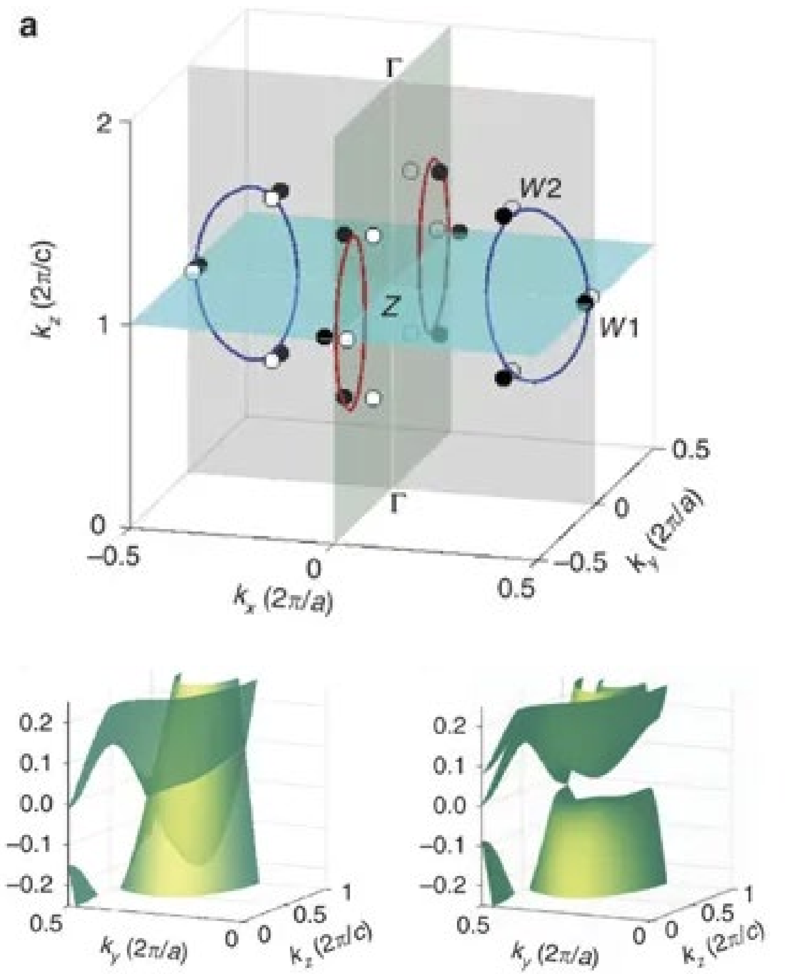

Huang et al., Nat. Com. (2016)

Type II Weyl semi metal

Minimal models for topological Weyl semimetals

Phys. Rev. B **95** 075133 2017.

Timothy M. McCormick,[1,*] Itamar Kimchi,[2,†] and Nandini Trivedi[1,‡]

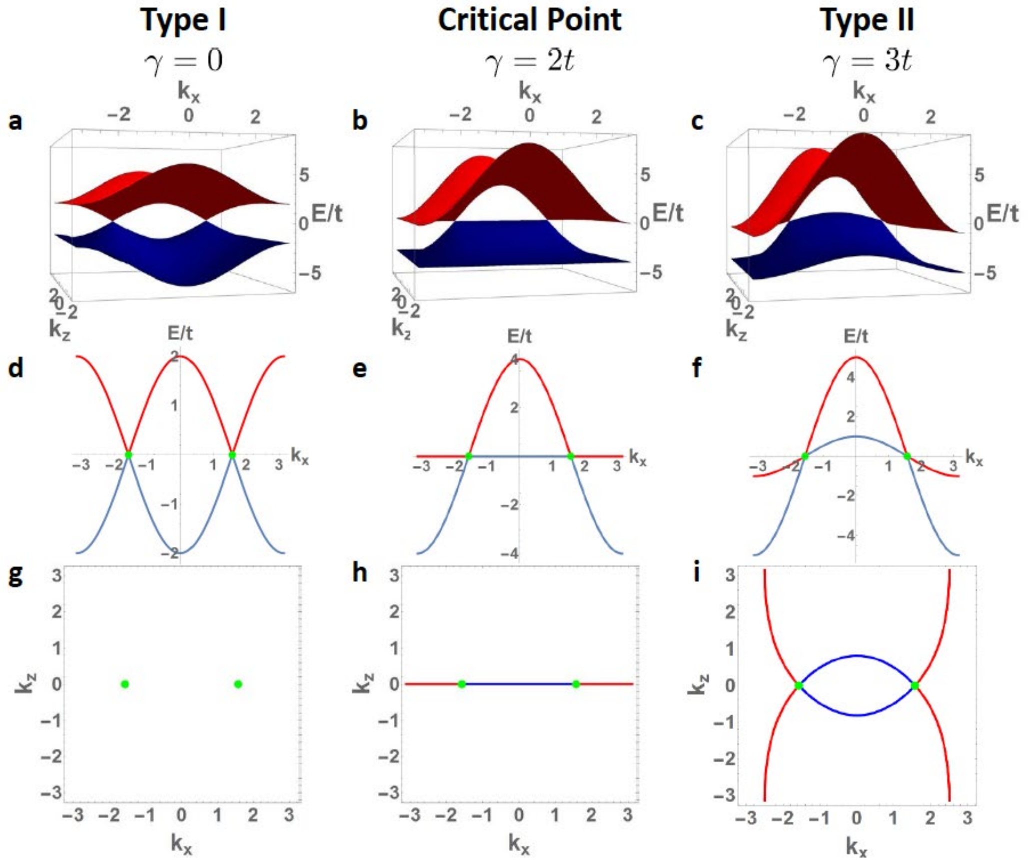

$$\hat{\mathcal{H}}_A^{\mathrm{TRB}}(\mathbf{k}) = \gamma\big(\cos(k_x) - \cos(k_0)\big)\hat{\sigma}_0 - \big(m(2-\cos(k_y)-\cos(k_z)) + 2t_x(\cos(k_x)-\cos(k_0))\big)\hat{\sigma}_1 - 2t\sin(k_y)\hat{\sigma}_2 - 2t\sin(k_z)\hat{\sigma}_3 \quad (8)$$

Chiral Anomaly: Weyl Fermions

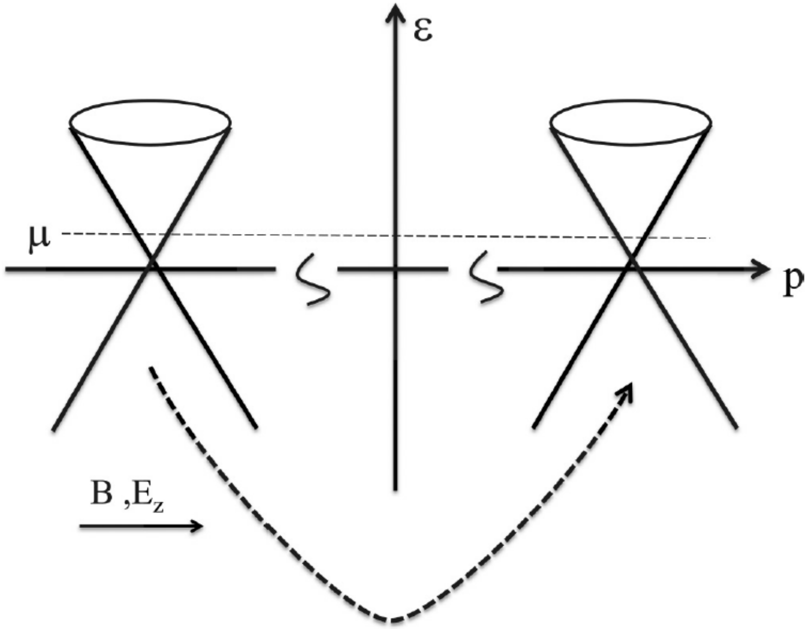

$$\sigma_{zz} = \frac{e^2}{4\pi^2\hbar c}\frac{v}{c}\frac{(eB)^2 v^2}{\mu^2}\tau.$$

Fukushima, Kharzeev, and Warringa
Phys. Rev. D 2008
Li et al, Nature Phys 2016

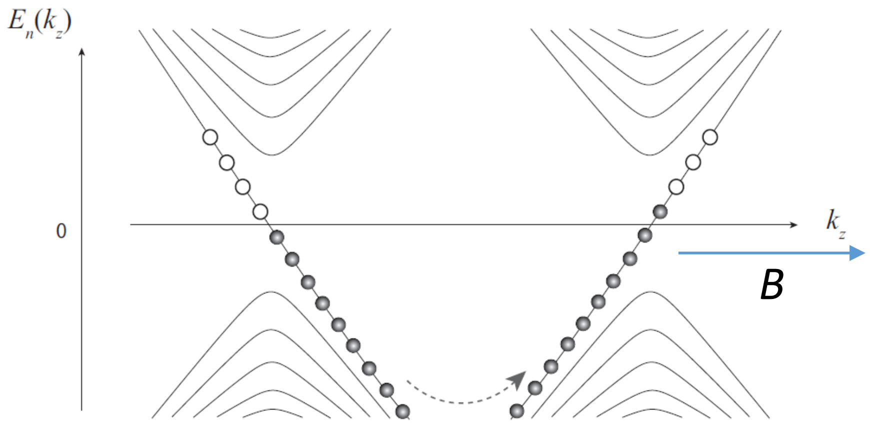

n = 0 Landau Level

Strongly Anisotropic Magnetoconductance
Only when *E//B*, Positive Magenetoconductance

D. T. Son and B. Z. Spivak, Phys. Rev. B **88**, 104412 (2013).

Chiral Anomaly: Weyl Fermions

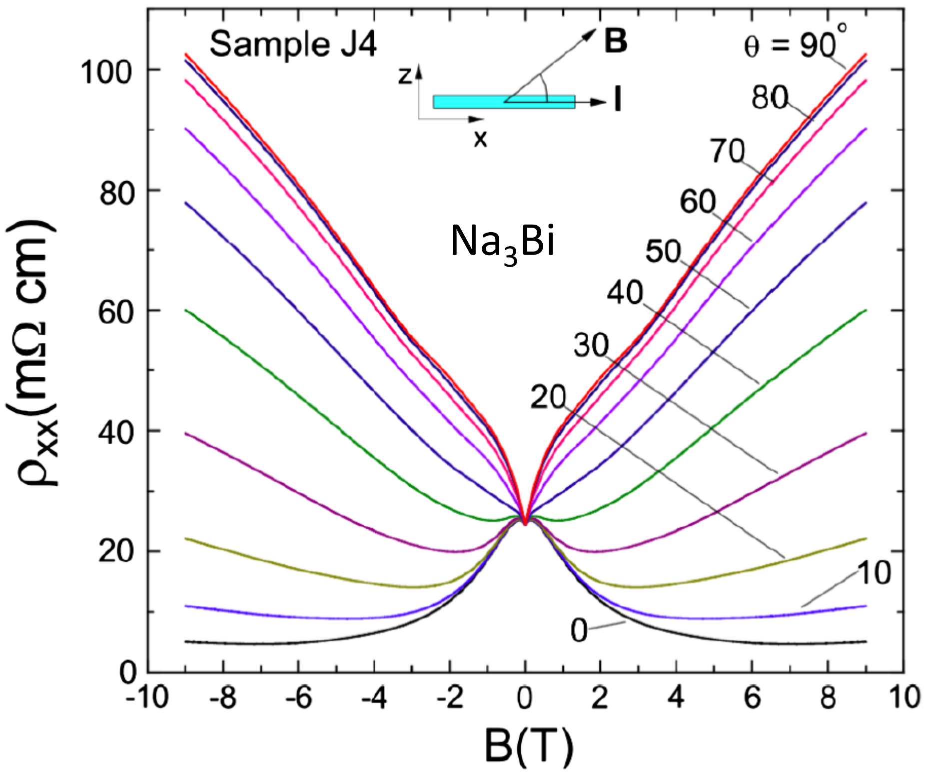

RESEARCH | REPORTS

Science 2015

TOPOLOGICAL MATTER

Evidence for the chiral anomaly in the Dirac semimetal Na_3Bi

Jun Xiong,[1] Satya K. Kushwaha,[2] Tian Liang,[1] Jason W. Krizan,[2] Max Hirschberger,[1] Wudi Wang,[1] R. J. Cava,[2] N. P. Ong[1]*

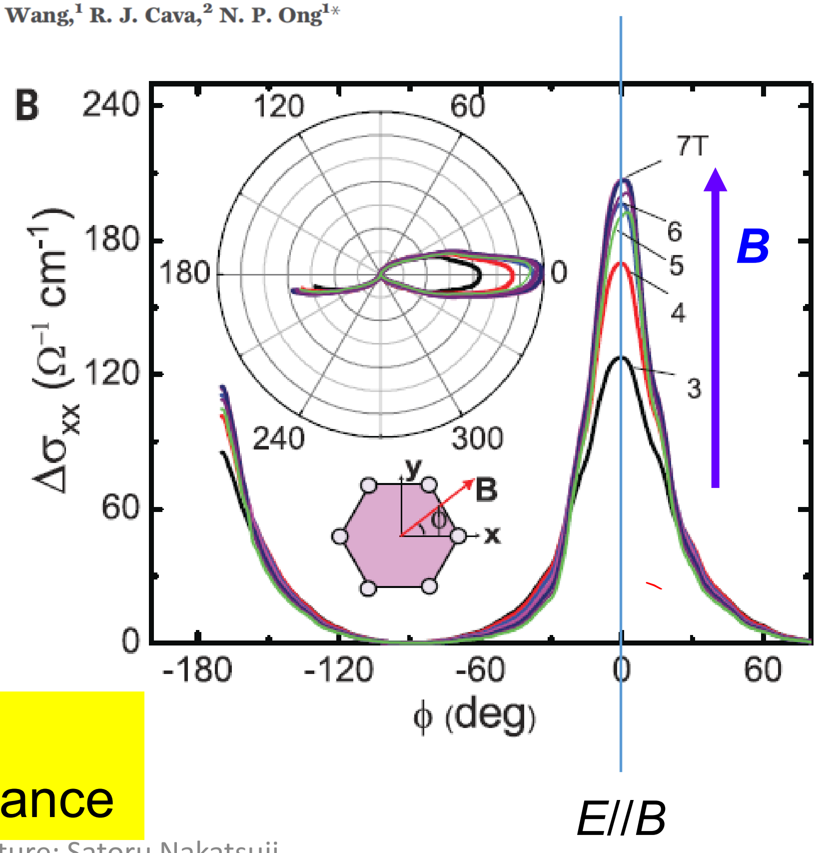

Strongly Anisotropic Magnetoconductance
Only when *E//B*, Positive Magenetoconductance

Magnetic Weyl Semimetals

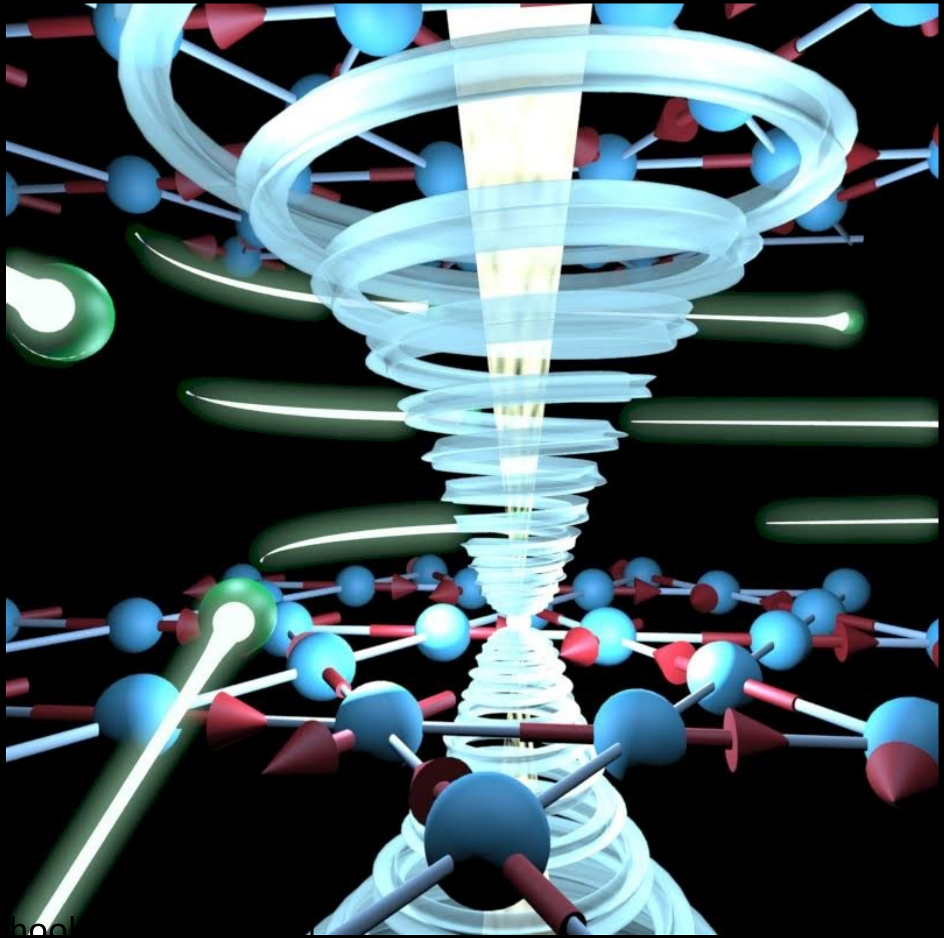

Weyl Magnets: Functional Magnets

Anomalous Hall Effect

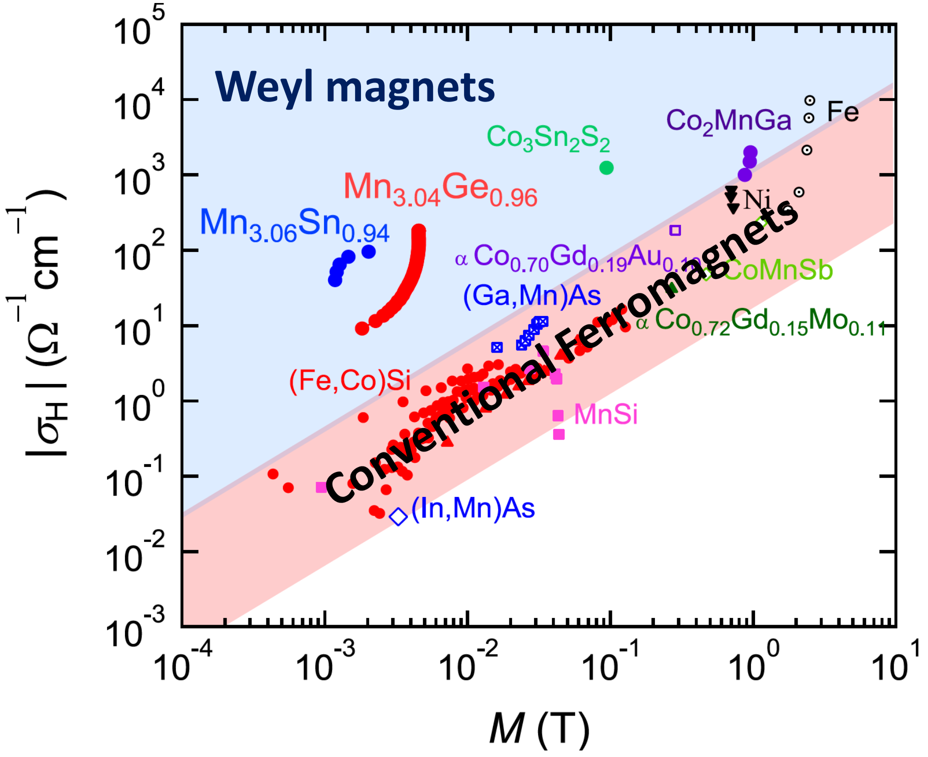

Anomalous Nernst Effect

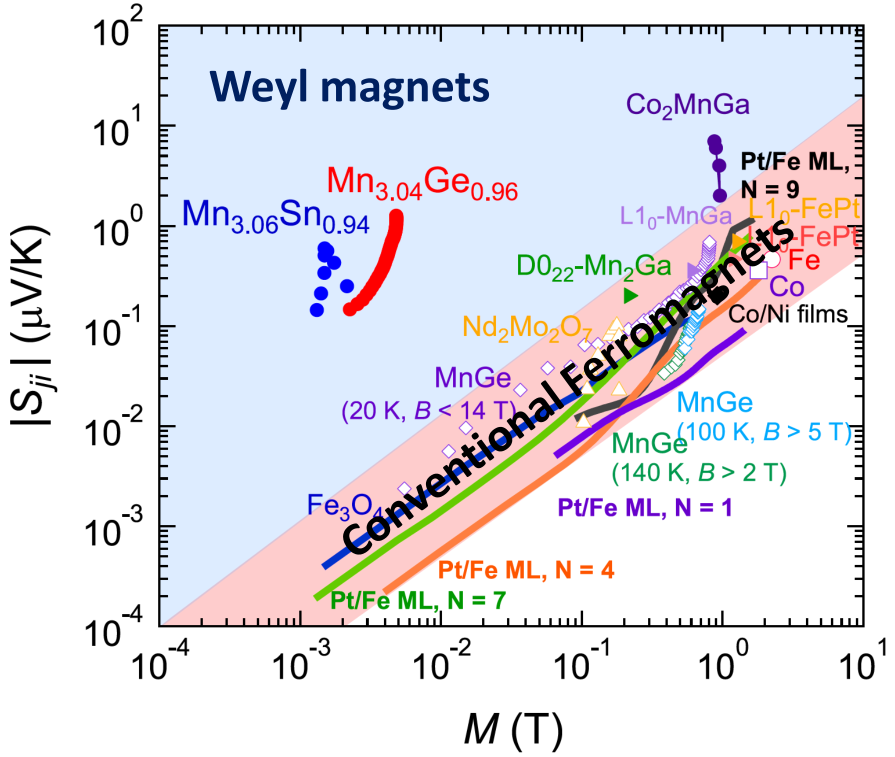

Non-volatile Memory

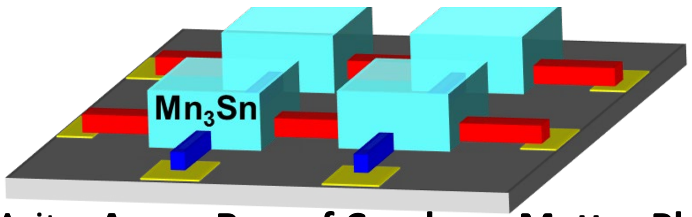

Thermoelectric Conversion

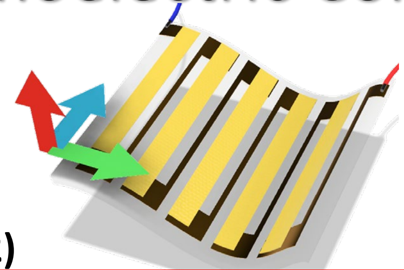

SN and R. Arita, **Annu. Rev. of Condens. Matter Phys., 13:119–42 (2022)**

Large responses are obtained irrespective of size of *M*.

Spontaneous Hall Effect in Spin Liquid

Pr^{3+} $4f^2$ non Kramers Ising moment
Ir^{4+} $5d^5$ conduction electron

AHE w.
***B* = 0**
***M* =0**

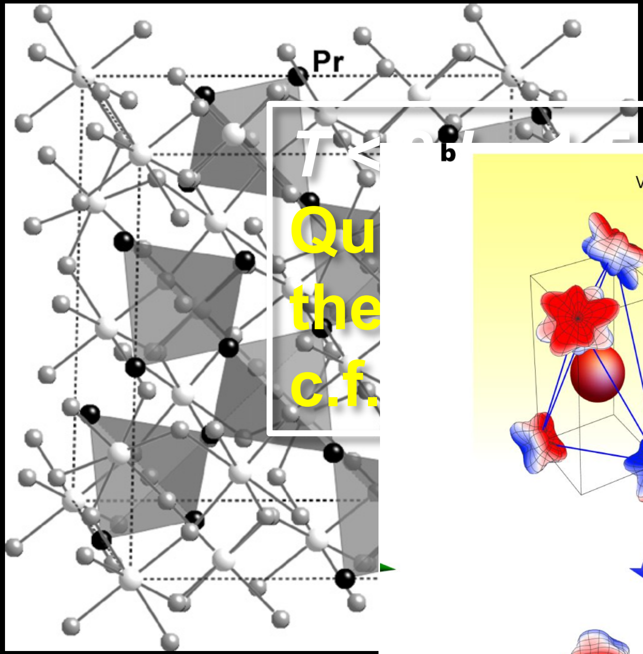

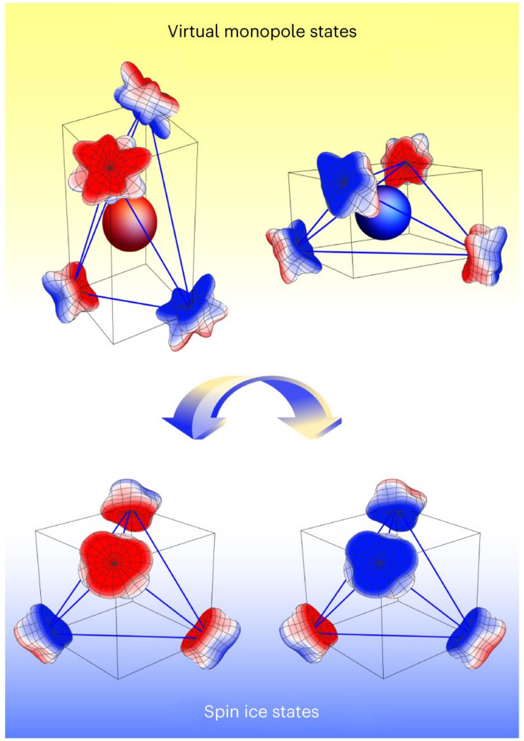

Spin-Orbital Liquid State
Tang et al., Nat. Phys. (2023).

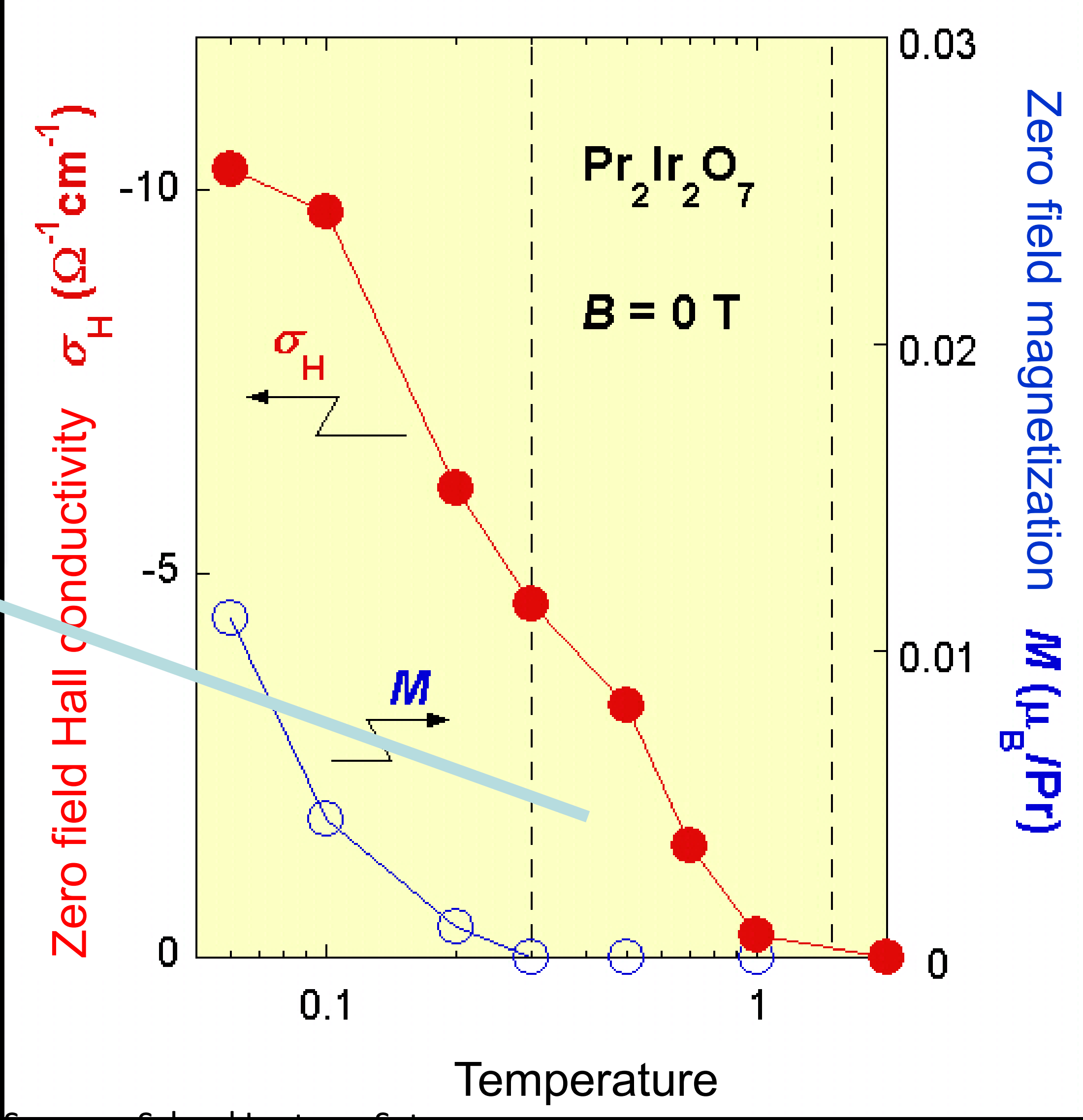

Quadrupolar moments (J_x & J_y) linearly couple to Strain ➔ Dynamical Jahn-Teller Effect

Machida et al., Nature (2009), Ohtsuki et al., PNAS (2019). cf. Guo et al., PRB (2020).

Spontaneous Hall Effect in Spin Liquid

Large Berry Curvature in *k*-Space

Large Hysteresis in Hall Effect

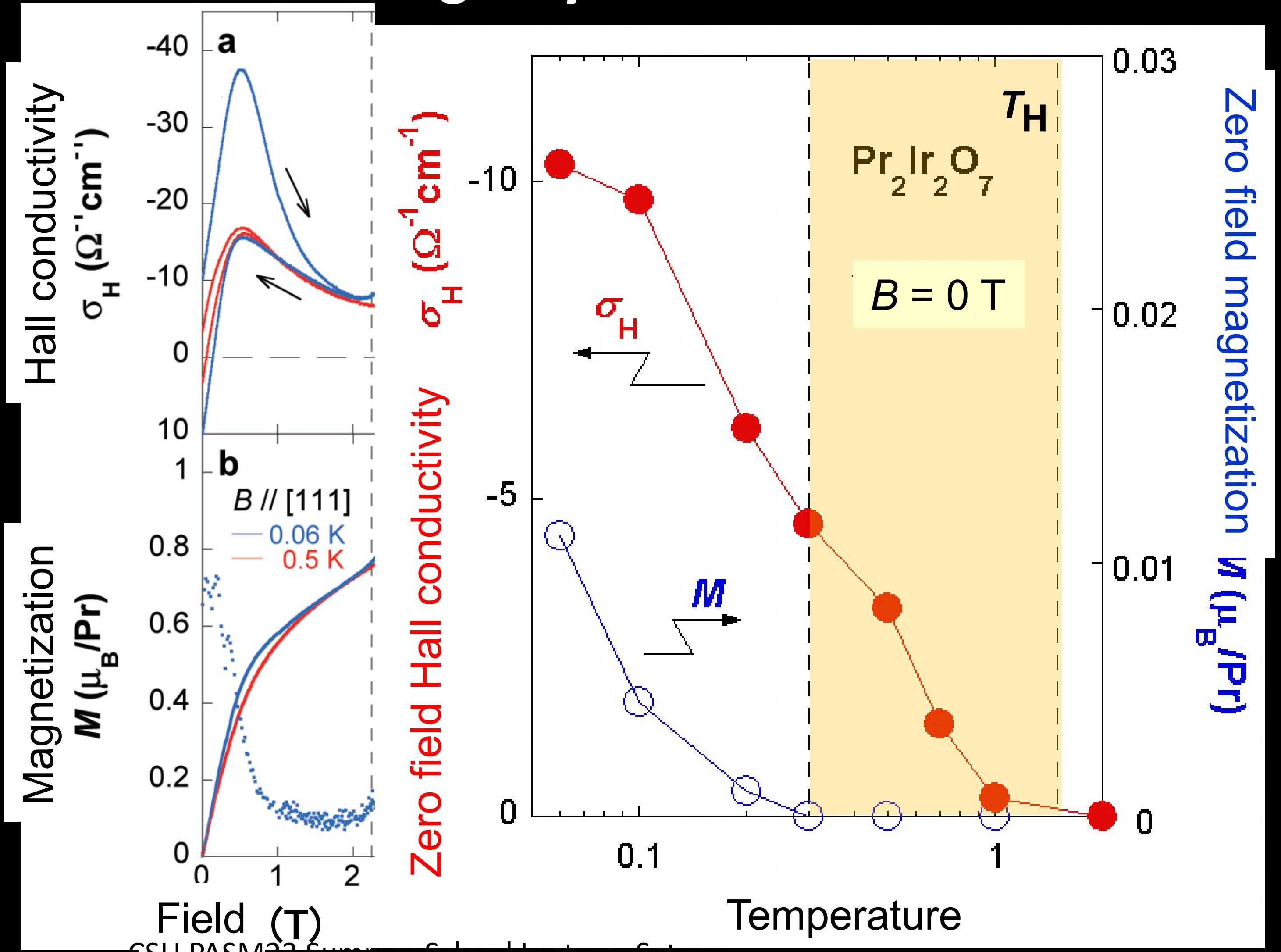

No Hysteresis in Magnetization

Machida et al., Nature (2009), Ohtsuki et al., PNAS (2019). cf. Guo et al., PRB (2020).

Platform for correlated topological semimetals

PHYSICAL REVIEW B **83**, 205101 (2011)

Topological semimetal and Fermi-arc surface states in the electronic structure of pyrochlore iridates

Xiangang Wan,[1] Ari M. Turner,[2] Ashvin Vishwanath,[2,3] and Sergey Y. Savrasov[1,4]

ry of Solid State Microstructures and Department of Physics, Nanjing University, Nanjing 210093, China

[2]*Department of Physics, University of California, Berkeley, California 94720, USA*

ls Sciences Division, Lawrence Berkeley National La

nt of Physics, University of California, Davis, One S

(Received 23 February 2011; publis

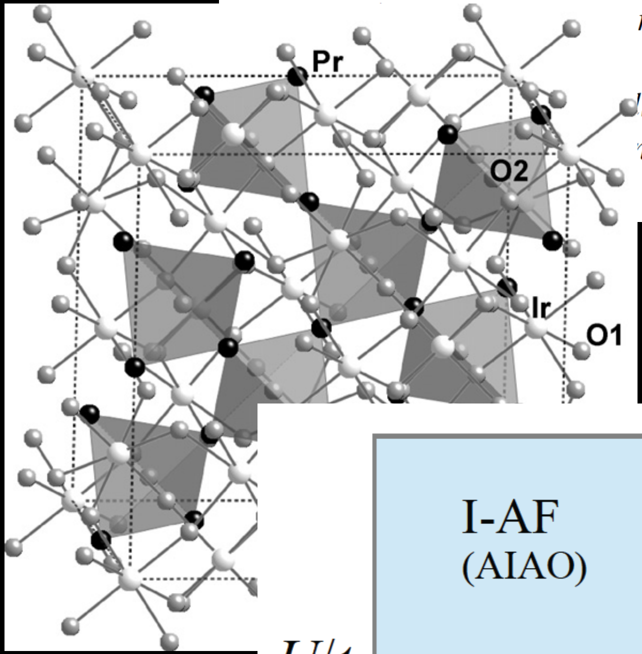

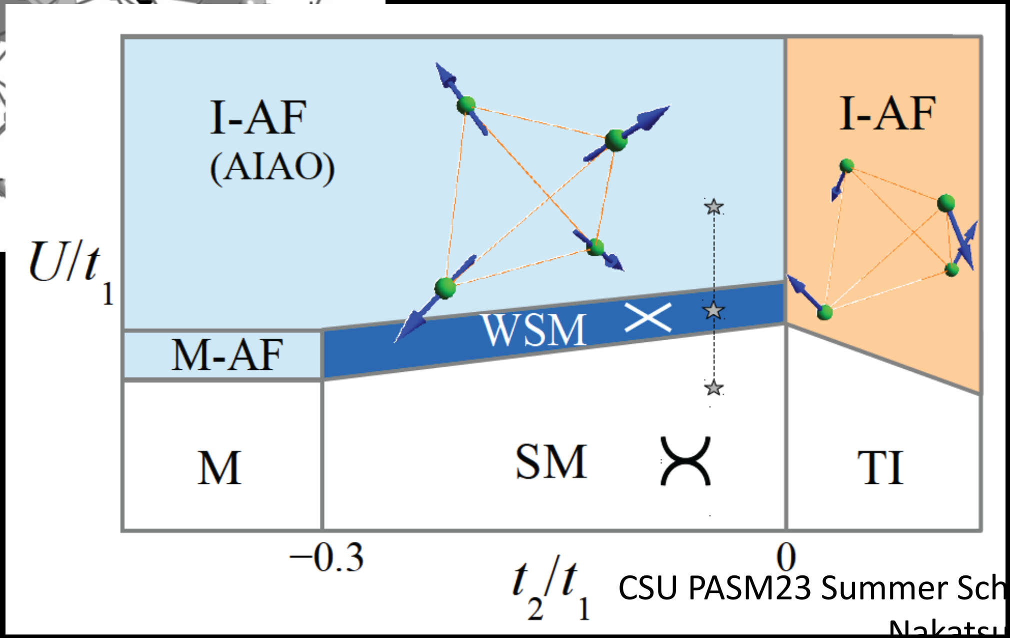

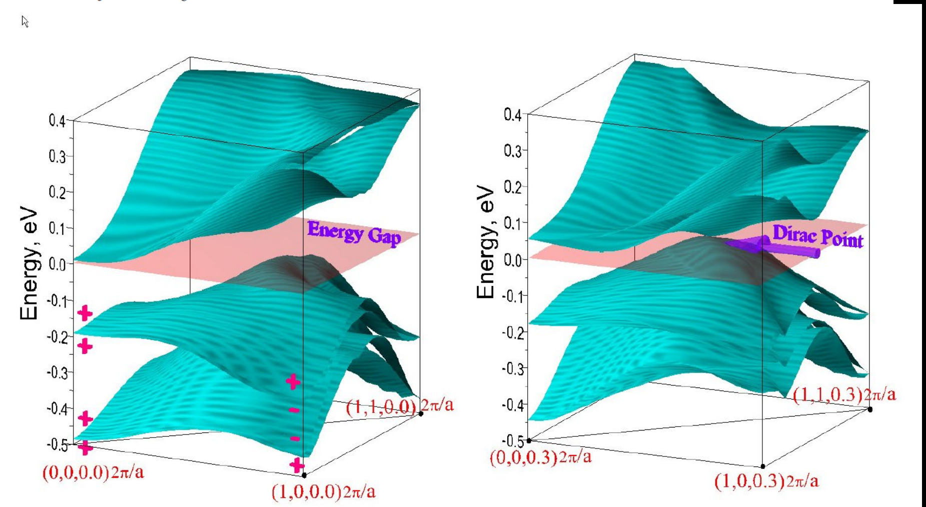

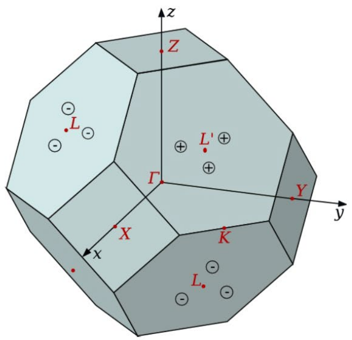

CSU PASM23 Summer Sch Lecture: Satoru Nakatsu

William Witczak-Krempa, Gang Chen, Yong Baek Kim, Leon Balents, Annu. Rev. Condens. Matter Phys. 5, 57, 2014.

Quadratic band touching: Luttinger Semimetal

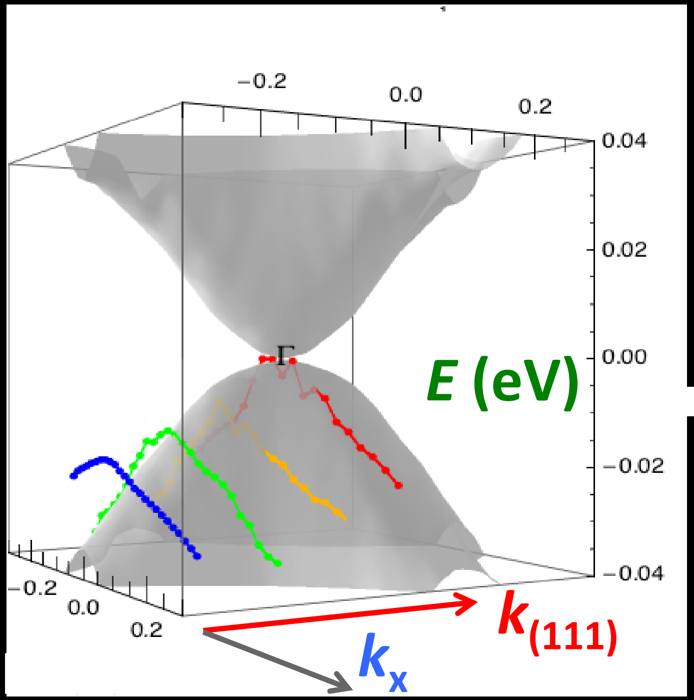

Exp. ARPES (UTokyo), THz (JHU+UTokyo)

Quadratic band touching at the Γ point

➔ Luttinger Hamiltonian

$$H = \frac{k^2}{2M_0} + \frac{\left(\frac{5}{4}k^2 - (\boldsymbol{k}\cdot\boldsymbol{J})^2\right)}{2m} - \sum_{i=x,y,z} \frac{k_i^2 J_i^2}{2M_c}$$

- ☐ Non-Fermi liquid due to the strong interaction.
- ☐ Touching points are not topologically protected
  - ➔ Parent states to various topological phases.
- ☐ Dielectric constant can be greatly enhanced.

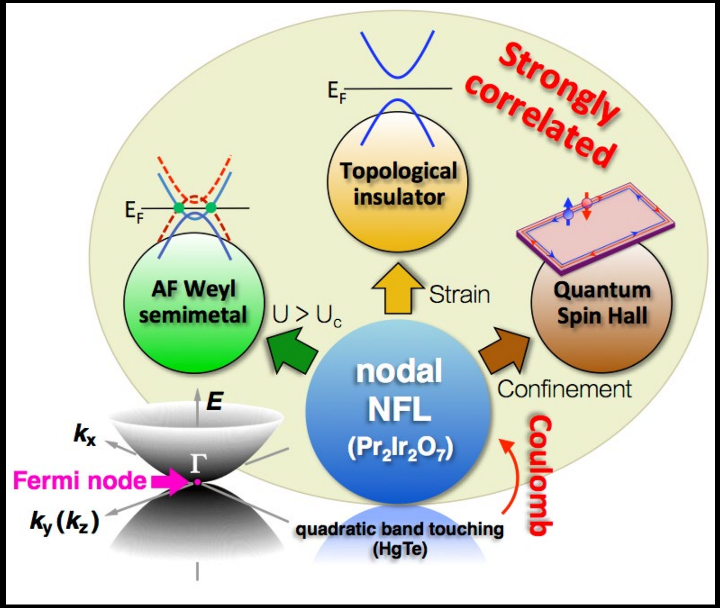

J. M. Luttinger (1956)., A. A. Abrikosov and S. D. Beneslavskii (1971).
A. A. Abrikosov (1974)., S. Murakami *et al.* (2004)., E.-G . Moon *et al.* (2013). T. Kondo, SN *et al.* (2015).

Zero field quantum criticality in $Pr_2Ir_2O_7$

Y. Tokiwa *et al.*, Nature Mat. **13**, 356 (2014).

Magnetic Grüneisen ratio ➔ divergence at field tuned QCP

$$\Gamma_H = -\frac{(\partial M/\partial T)_H}{C} = -\frac{1}{T}\frac{(\partial S/\partial H)_T}{(\partial S/\partial T)_H} = \frac{1}{T}\left(\frac{\partial T}{\partial H}\right)_S$$ = magnetocaloric effect

[8] M. Garst *et al.*, PRB **72**, 205129 (2005). [9] L Zhu *et al.*, PRL **91**, 066404 (2003).

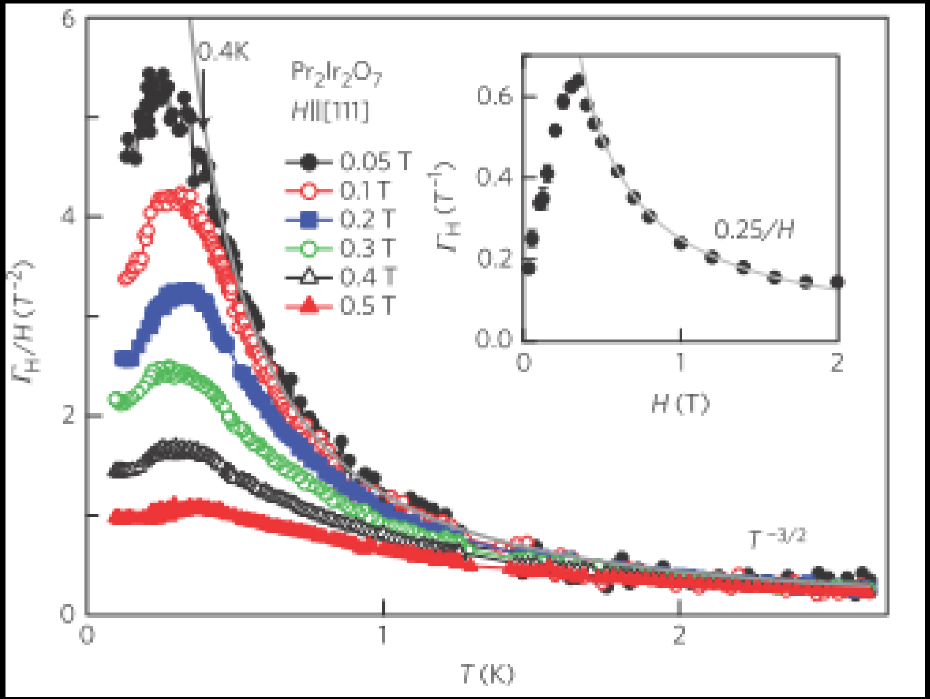

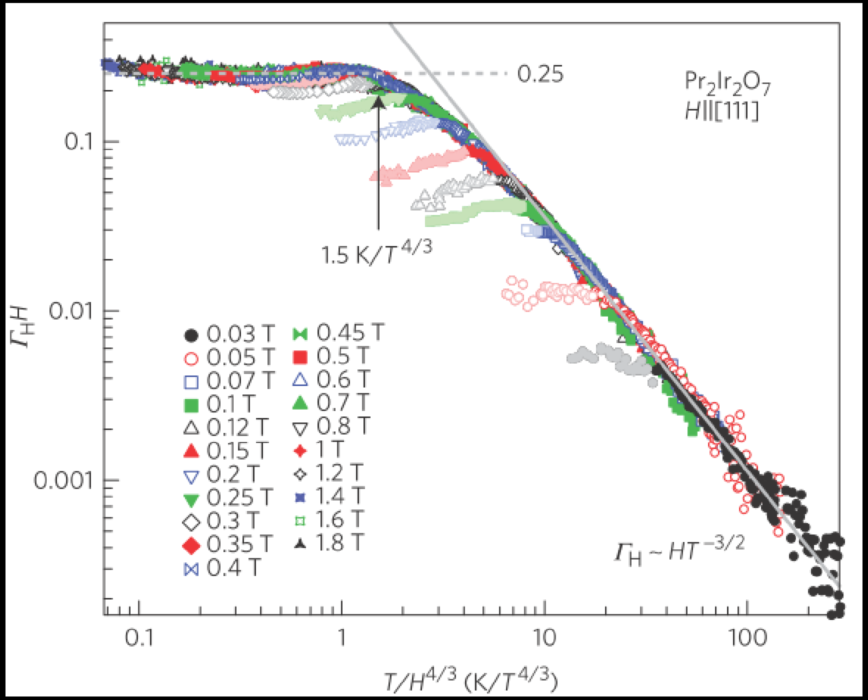

- Diverging Γ_H @ $H \to 0$ down to 0.4 K as $\Gamma_H \propto HT^{-3/2}$
- Scaling behavior in $T/H^{4/3}$ without critical field. ➔ zero field quantum critical point

Correlated topological semimetal

Various topological phases in correlated matter:
key observations: spontaneous Hall effect

- Nonmagnetic/paramagnetic systems
  - Topological Non-Fermi Liquid: ex $Pr_2Ir_2O_7$
  - Weyl Kondo Semimetal: ex $Ce_3Bi_4Pd_3$

- Magnetic Systems
  - Quantum Anomalous Hall Effect ex Mag. Doped TI
  - Ferromagnetic Weyl semimetals: ex Co_2MnGa, $Co_3Sn_2S_2$
  - **Antiferromagnetic Weyl semimetal: ex Mn_3Sn**

Topological Antiferromagnets for Spintronics

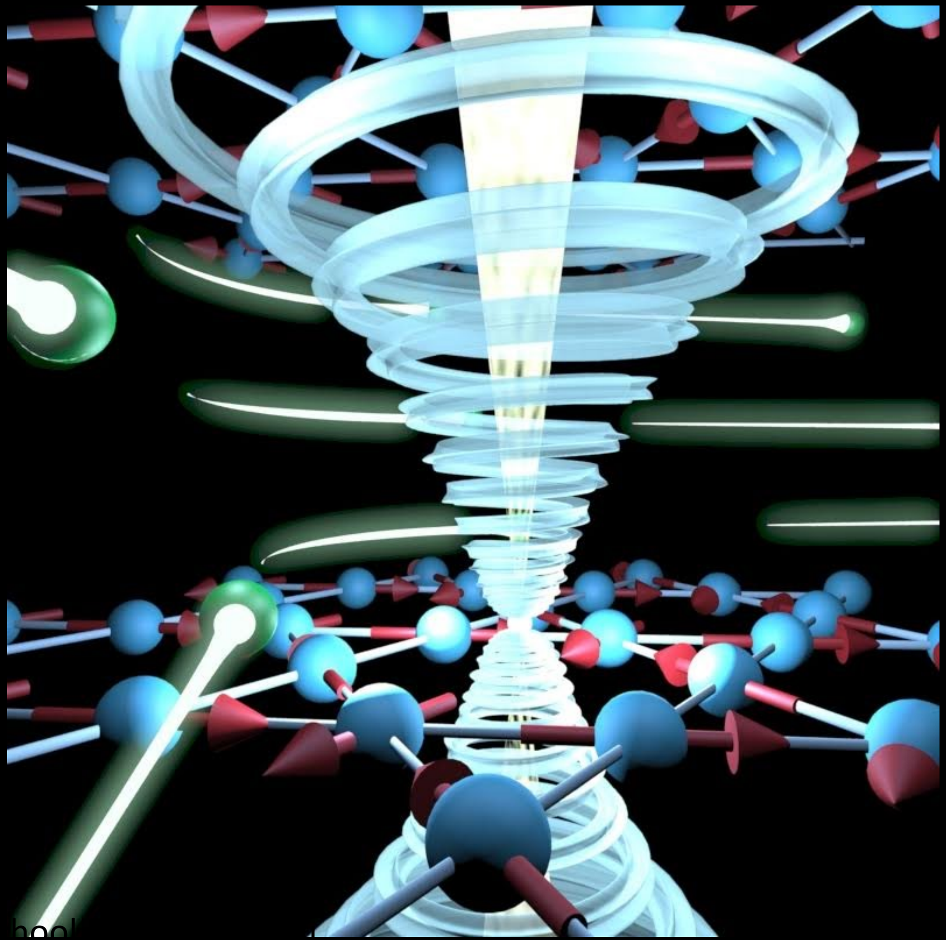

Antiferromagnetism: Spintronicis

- *Produce no stray fields*
- *Robust against perturbation due to field*
- *Ultrafast dynamics (~ THz)(cf. FM ~ GHz)*

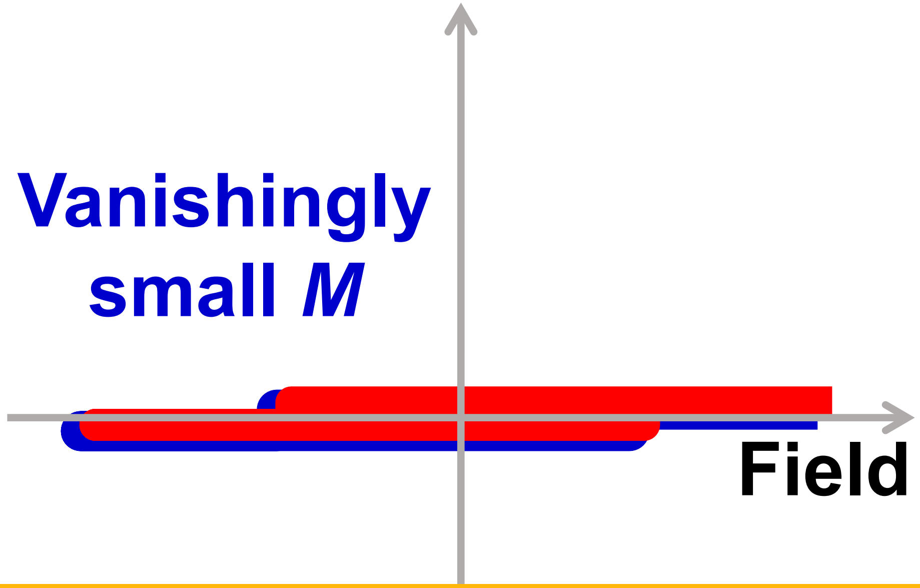

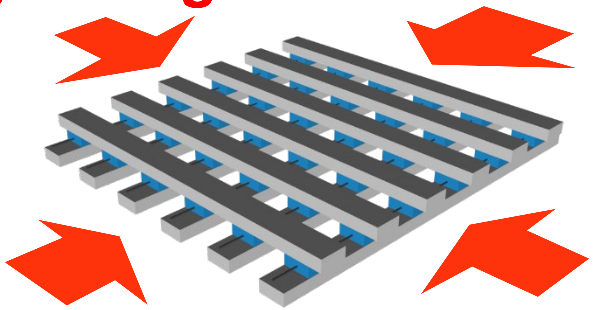

Hard to control, Small response

Topo. Functional Magnet Mn_3X

Large Response as in FMs

Vanishingly small *M*

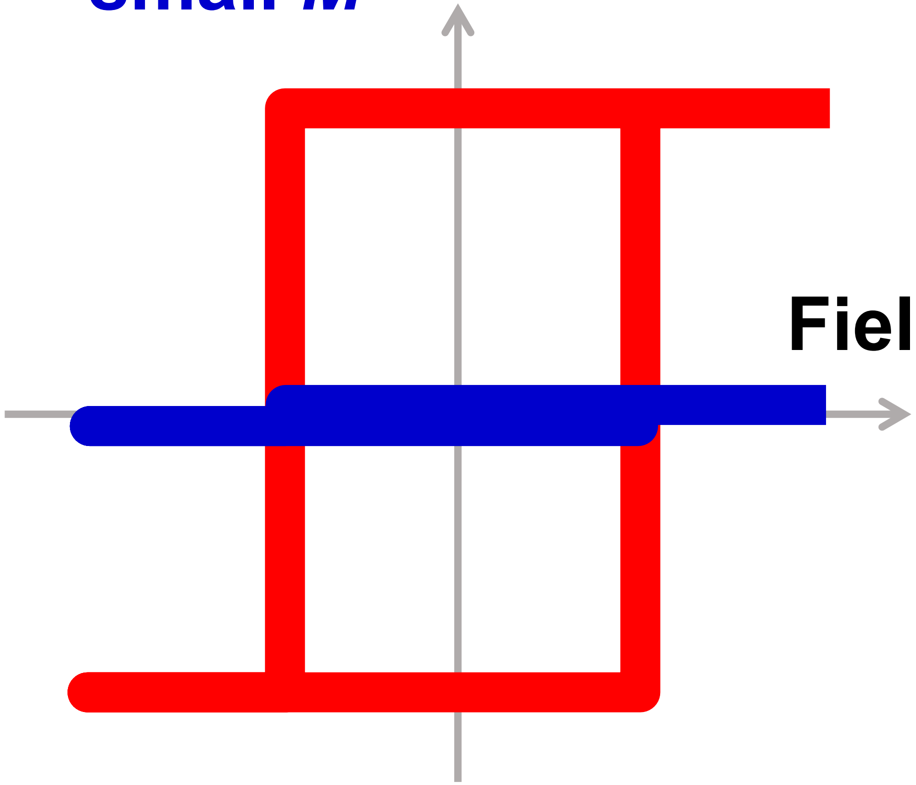

Dynamics ~THz

Topological Weyl AFM

Mn_3Sn

Multipole

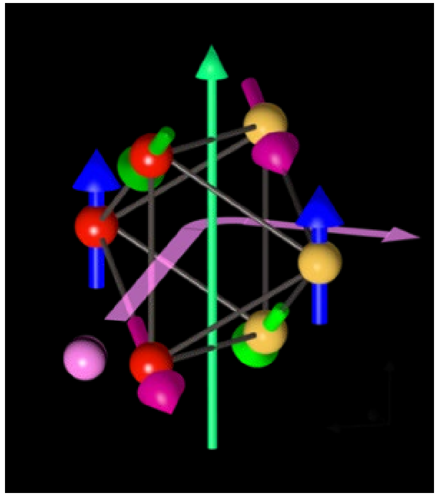

Real Space

Weyl Points

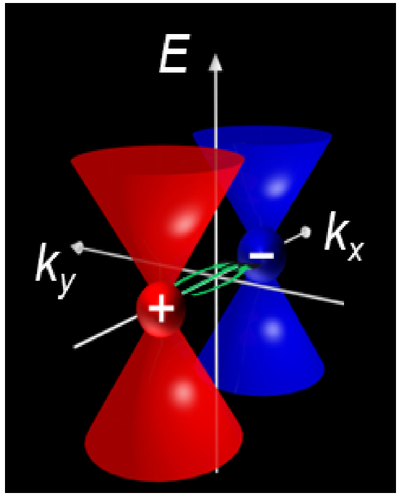

Momentum Space

Electrical Manipulation

*Tsai⁺, Higo⁺ et al., Nature **580**, 608 (2020).*

- **Electrical Switching of a Weyl Semimetallic State**

✓ **Antiferromagnets**

✓ **The same protocols as in FMs**

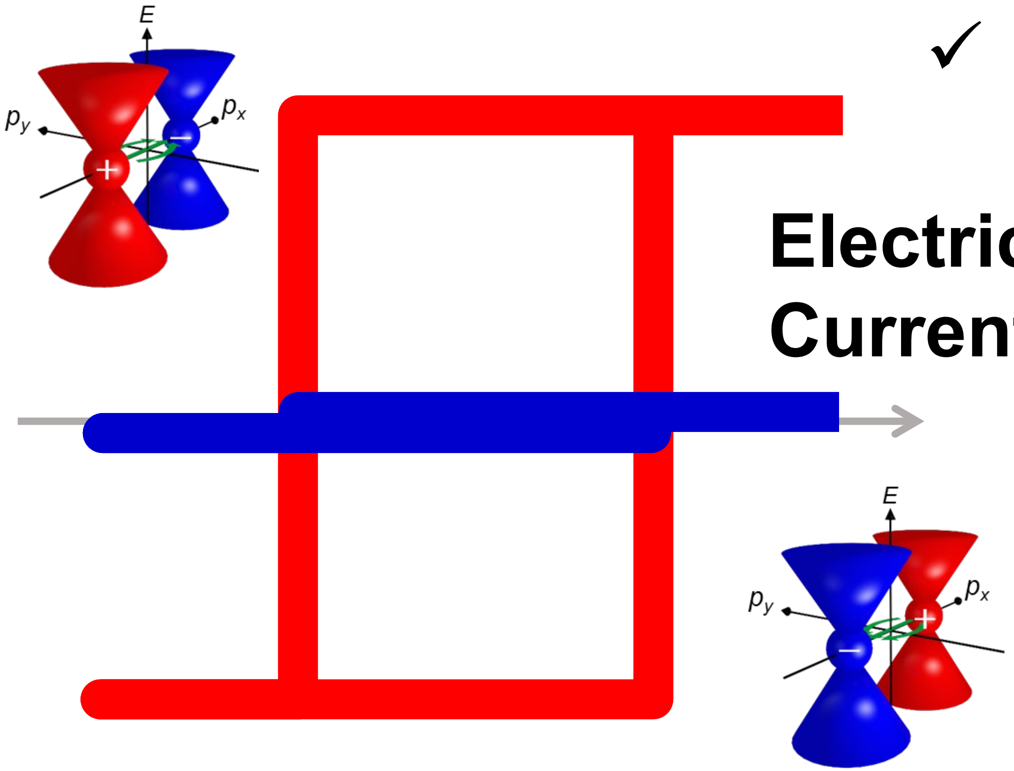

- Hall bar devices in AF Weyl SM

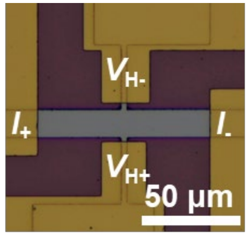

⇔ 8-term. for collinear AFMs

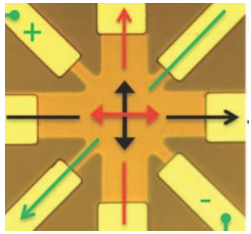

P. Wadley *et al.*, Science **351**, 587 (2016).

Weyl Semimetallic State in Mn_3Sn

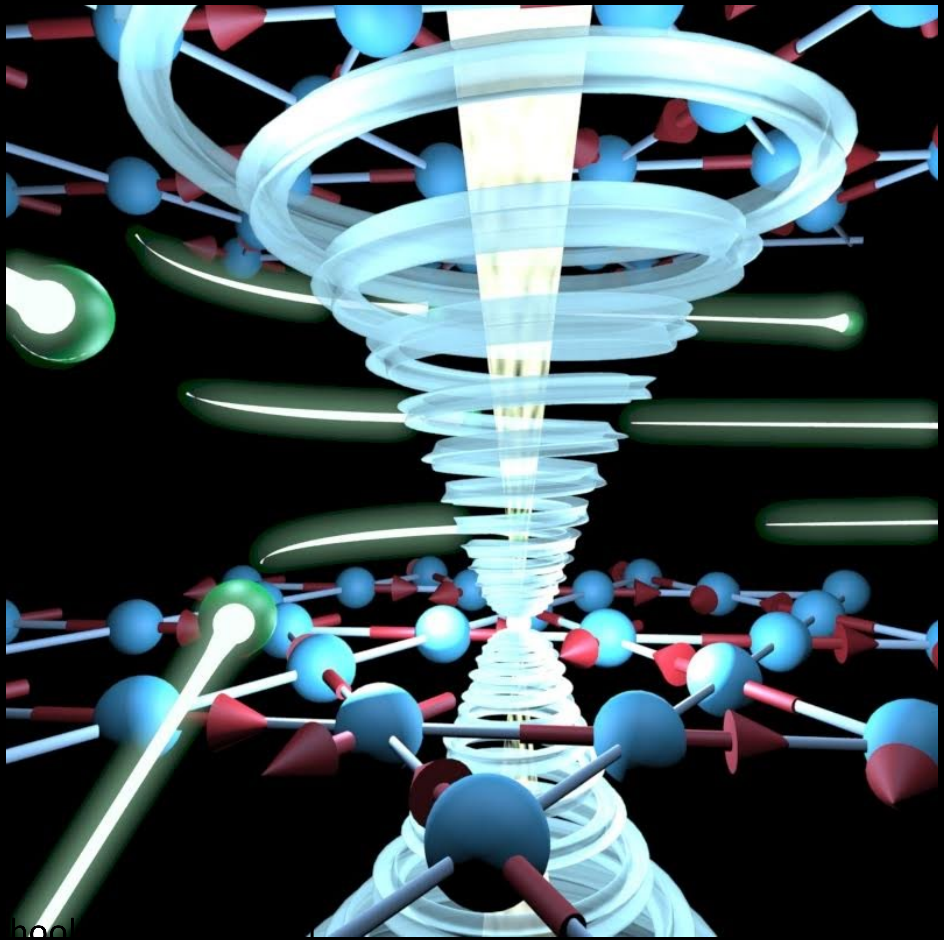

Kagome Weyl AFM Mn_3X (X = Sn, Ge)

Chiral antiferromagn

@T_N = 430 K

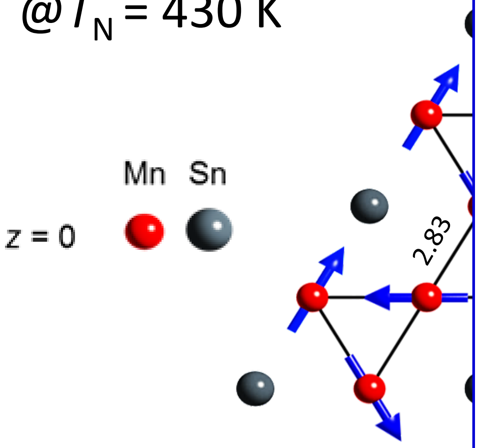

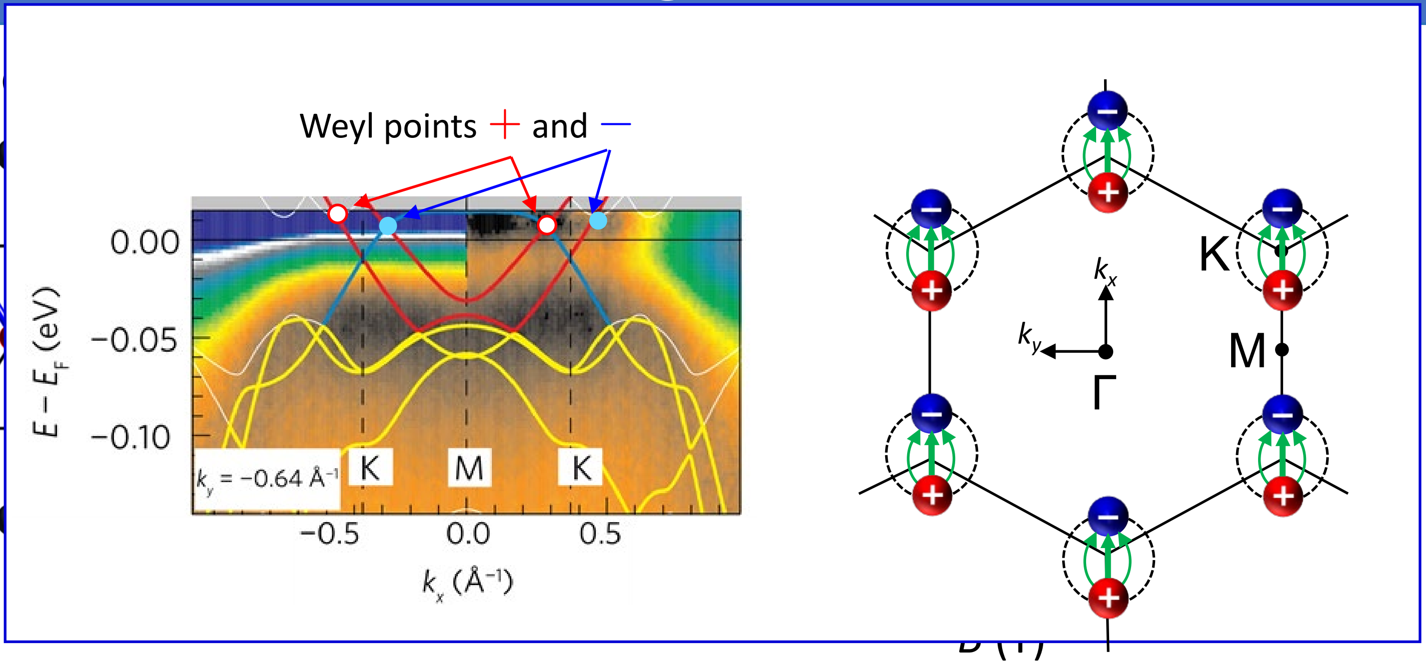

Despite the small spontaneous magnetic moment ~ $\mathrm{m}\mu_B$,

large AHE is observed, comparable to the one in FM.

Weyl points close E_F w/ Strong correlation, Large Renormalization

S. N., N. Kiyohara, T. Higo, *Nature* (2015)., N. Kiyohara *et al.*, *Phys. Rev. Applied* (2016).
M. Ikhlas, T. Tomita, *et al.*, *Nature Physics* (2017).
K. Kuroda, T. Tomita, *et al.*, *Nature Materials* (2017). , T. Higo *et al*. *Nature Photon*. (2018).
Theory: Hua Chen et al. PRL (2014).

Chiral Anomaly in Antiferromagnets Mn_3Sn & Mn_3Ge

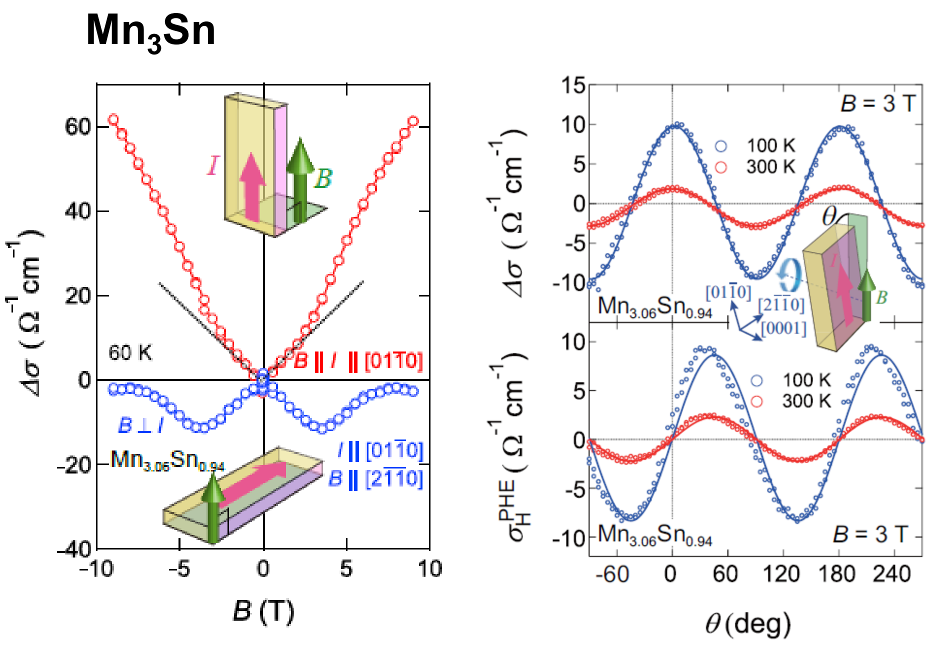

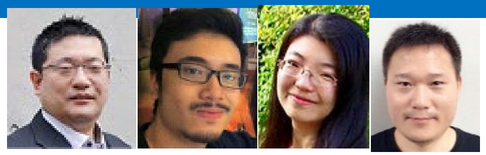

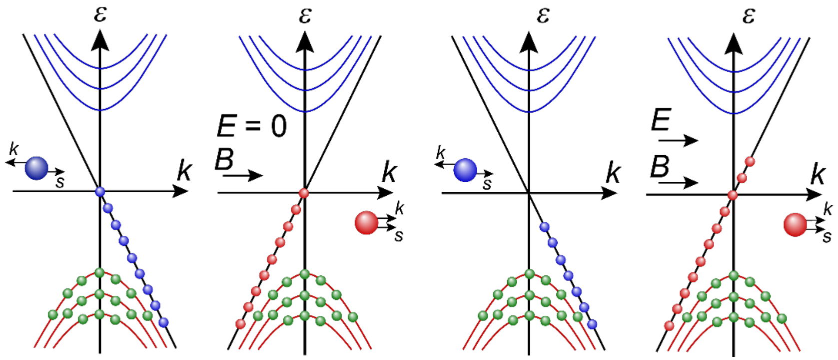

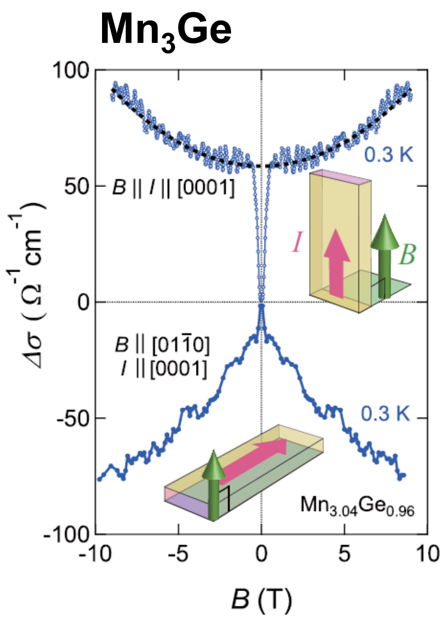

Chiral anomaly through the MC and PHE

Magnetoconductance $\Delta\sigma = \Delta\sigma_{\text{chiral}} \cos^2\theta$

Planar Hall Effect $\Delta\sigma_{\text{H}}^{\text{PHE}} = \Delta\sigma_{\text{chiral}} \sin\theta \cos\theta$

Kuroda, Tomita, Kondo, SN *et al.*, *Nature Materials* (2017).
Chen, Tomita, Minami, Fu, SN *et al., Nature Commun*. (2021).

Nernst Effect vs. Magnetization

Nat. Phys. 2017

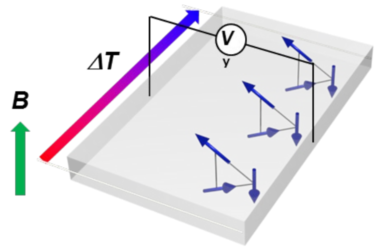

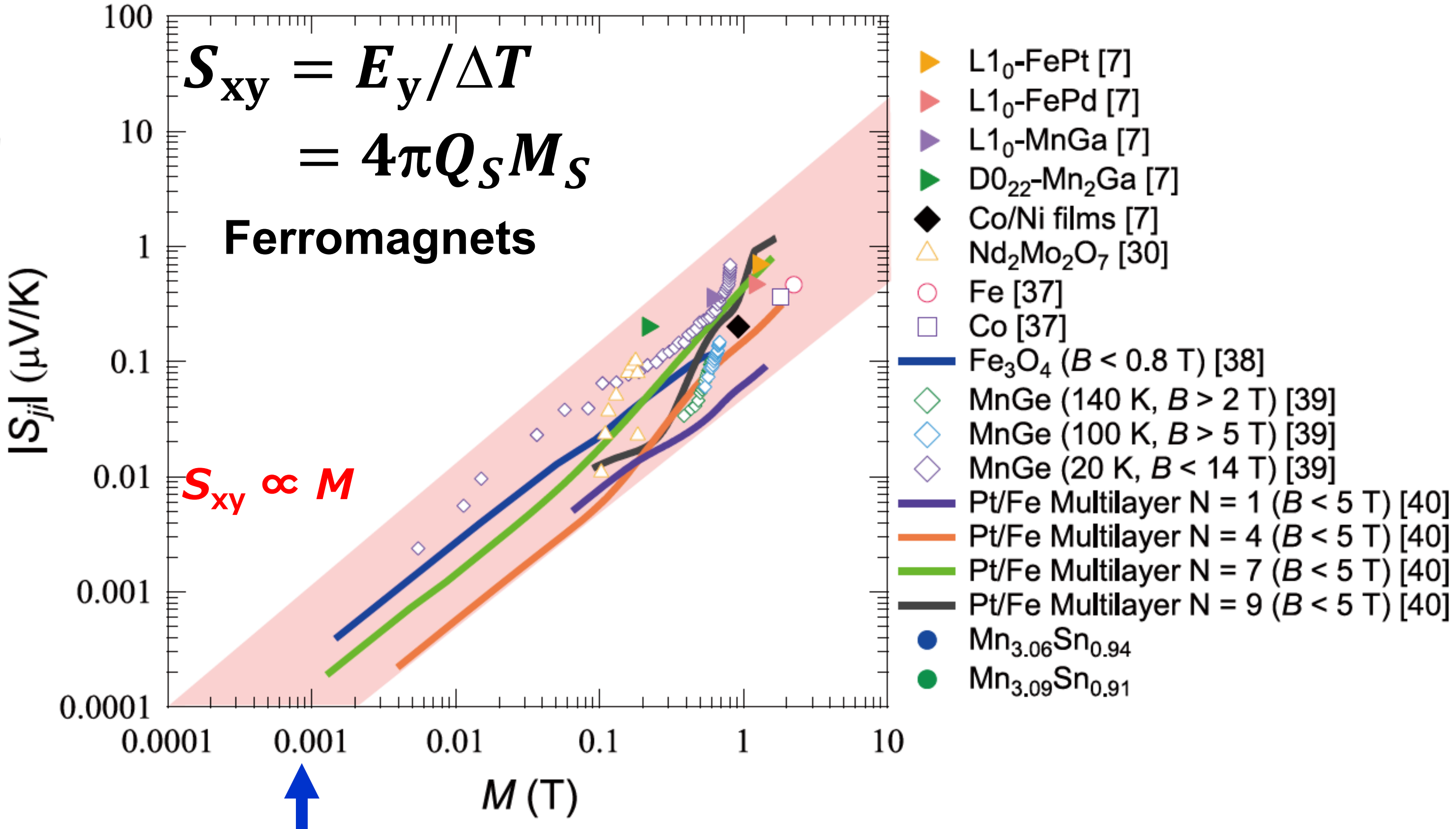

AFM Mn_3Sn

Nernst Effect vs. Magnetization

Nat. Phys. 2017

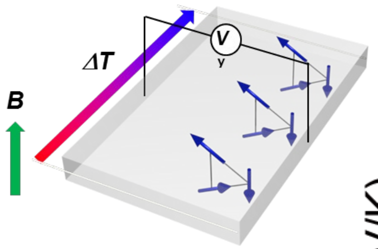

Ikhlas, Tomita et al., Nature Phys. (2017).

X. Li et al
PRL **119**, 056601 (2017).

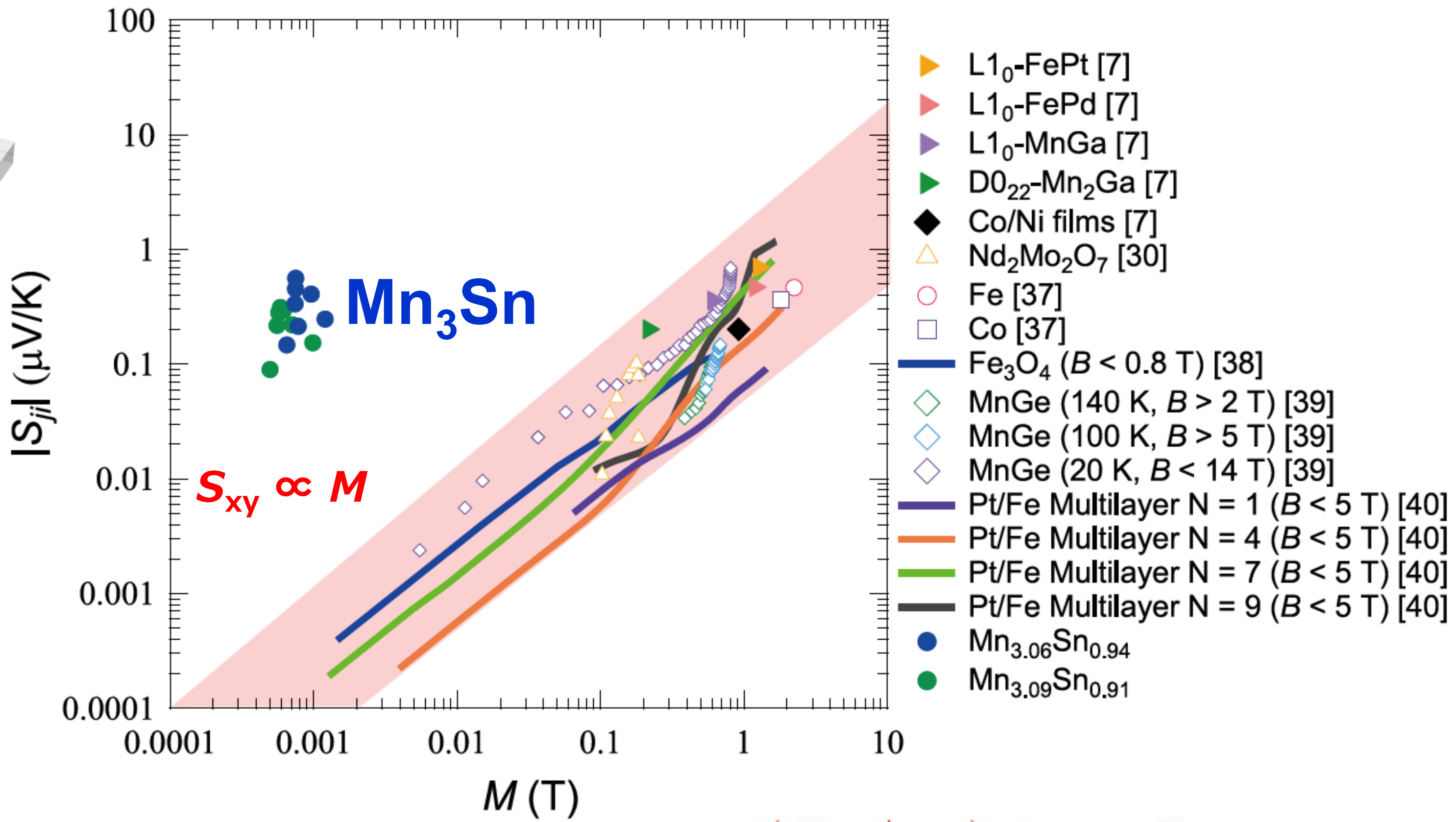

Transverse Thermoelectric Conductivity $\alpha_{zx} = (S_{zx}/\rho_{zz}) + \sigma_{zx} S_{xx}$

$$\alpha_{zx} = -\frac{e}{T\hbar}\int \frac{d\boldsymbol{k}}{(2\pi)^3}\Omega_{n,y}(\boldsymbol{k})\left\{(\varepsilon_{n\boldsymbol{k}}-\mu)f_{n\boldsymbol{k}} + k_{\mathrm{B}}T\ln\left[1+e^{-\beta(\varepsilon_{n\boldsymbol{k}}-\mu)}\right]\right\}$$

■Nernst Effect：~Berry curvature at Fermi Energy

100～1000 times more than ferromagnets

Large Berry Curvature near E_F

Mn_3Sn, Weyl Magnet

Control of Fictitious Field of a few 100 T by External Magnetic Field of 100 G.

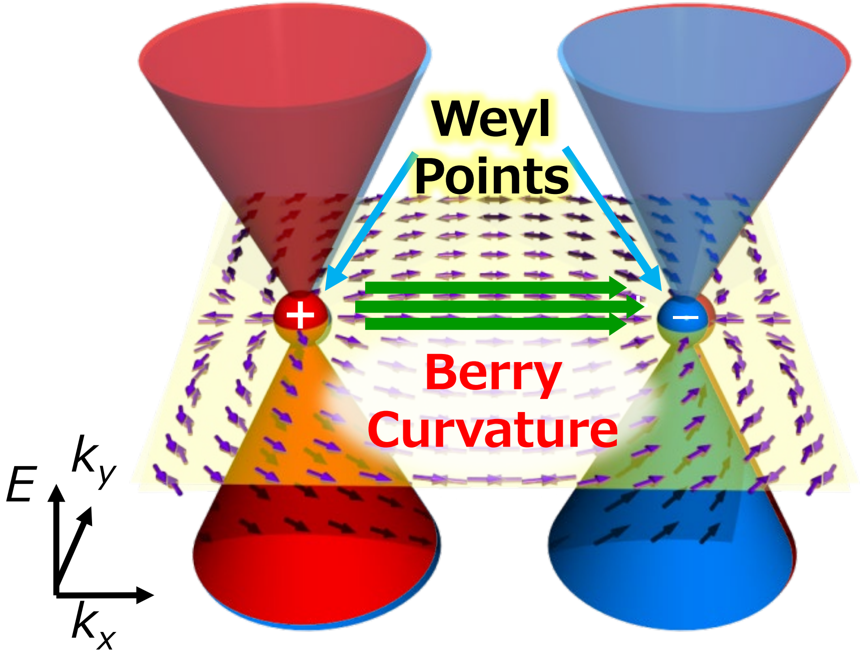

Nature Materials (2017).

$$\sigma_{xy} = n\frac{e^2}{\hbar}\langle\Omega\rangle$$

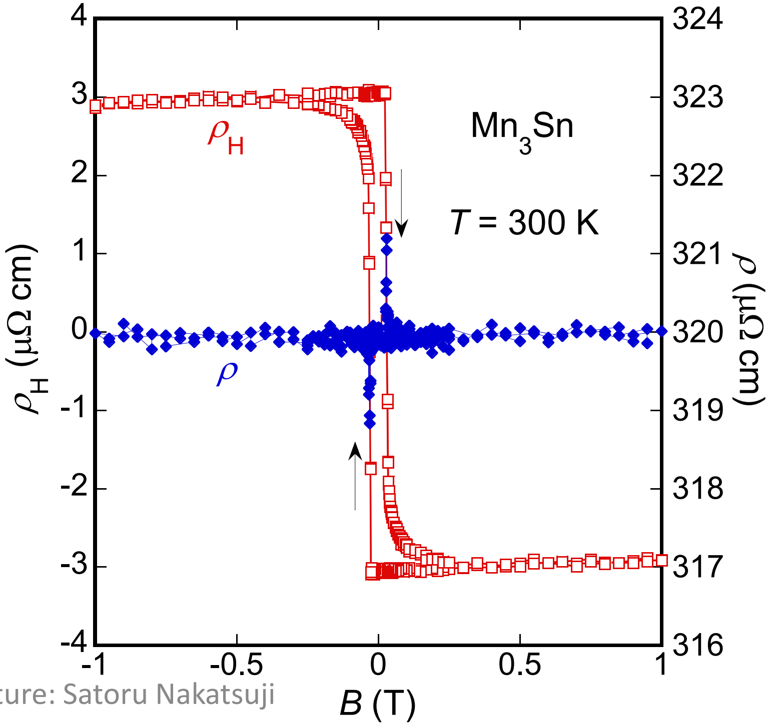

Control of Weyl Points

Control of Fictitious Field of a few 100 T by External Magnetic Field of 100 G.

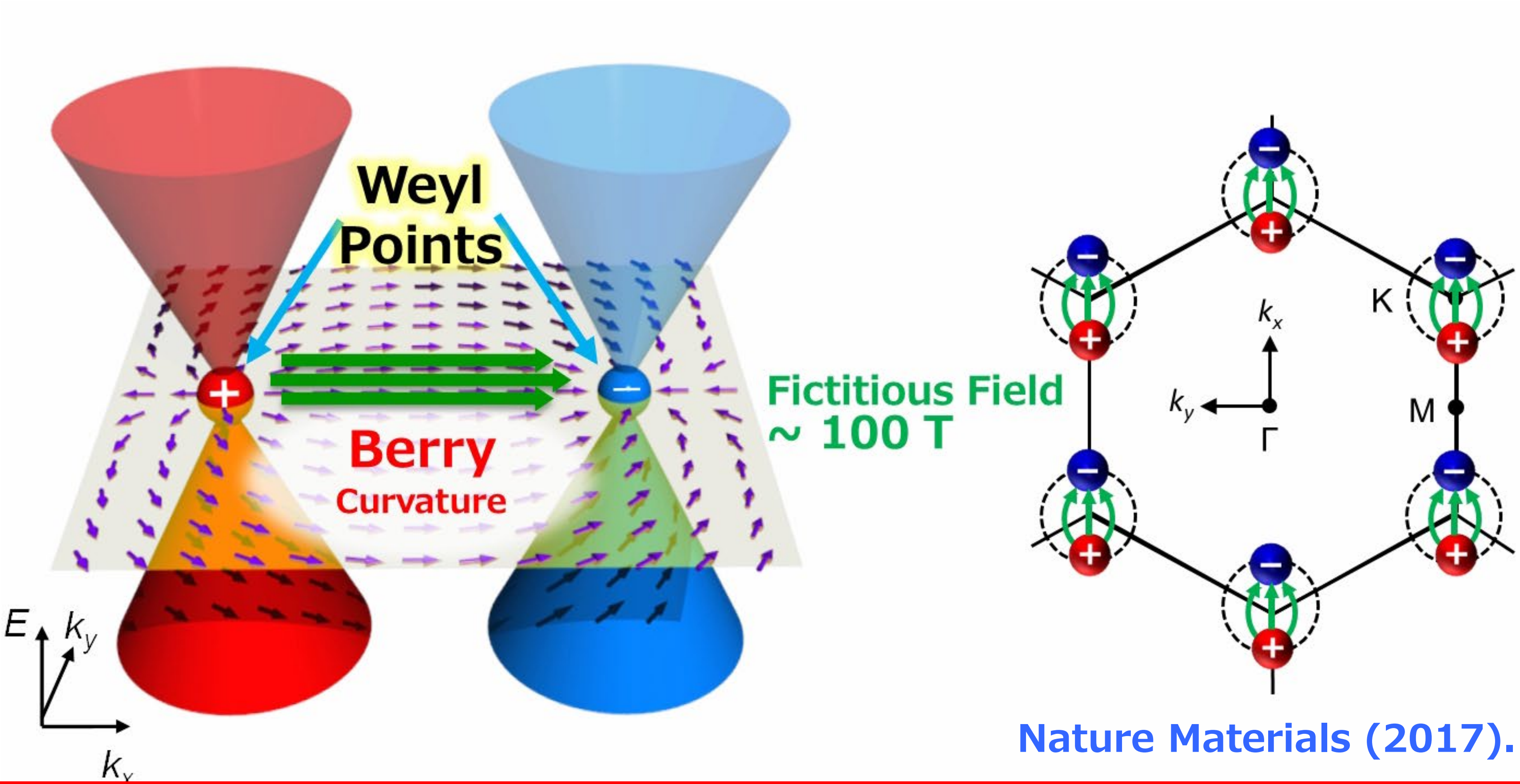

Nature Materials (2017).

Manipulation of Weyl Points is useful for AF Spintronics

Electrical Manipulation of Weyl Semimetallic State in Mn_3Sn

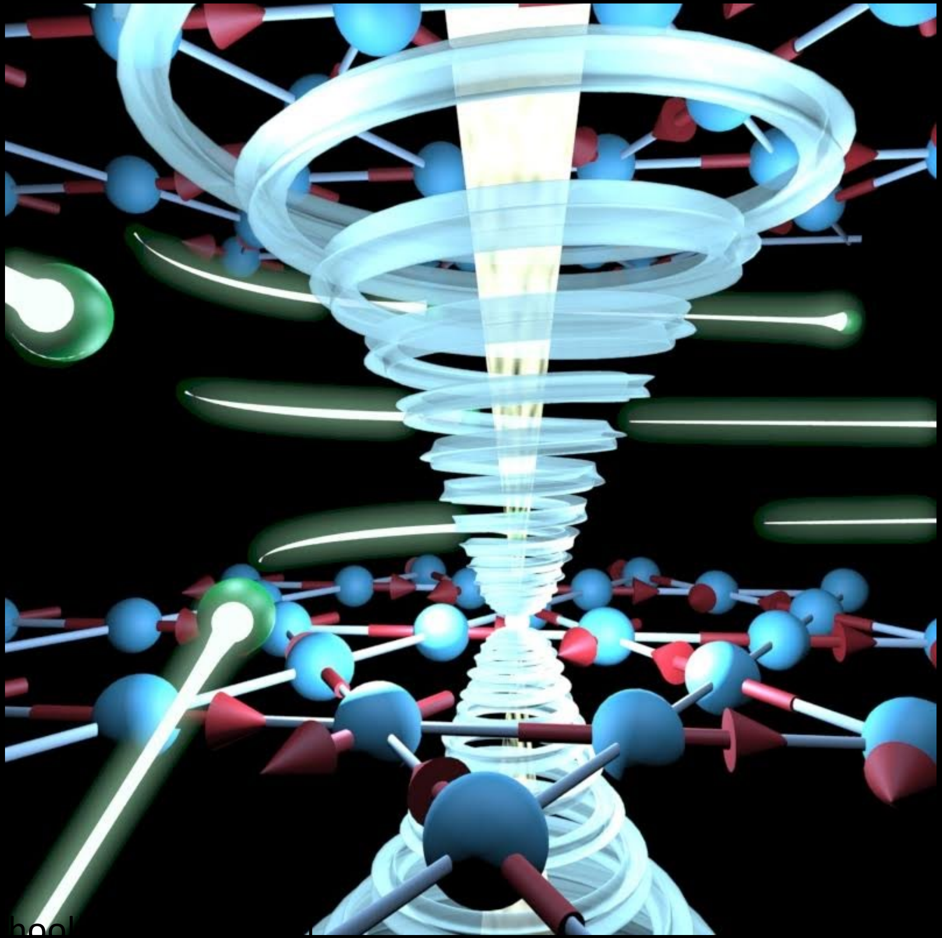

Evidence for Weyl semimetal in Mn_3Sn films

*Tsai⁺, Higo⁺ et al., Nature **580**, 608 (2020).*

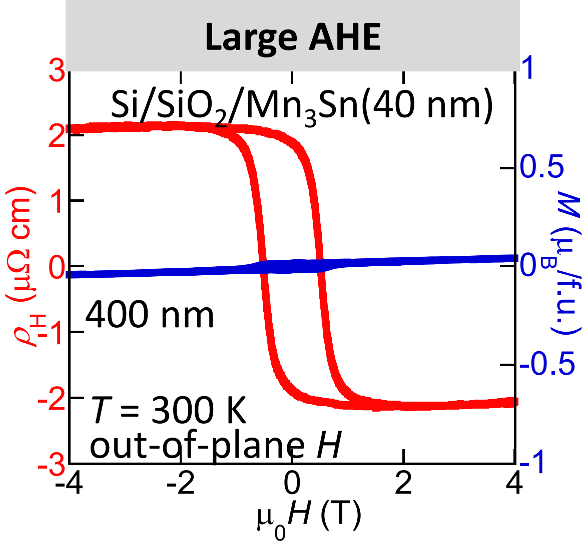

*Higo et al., APL **113**, 202402 (2018).*

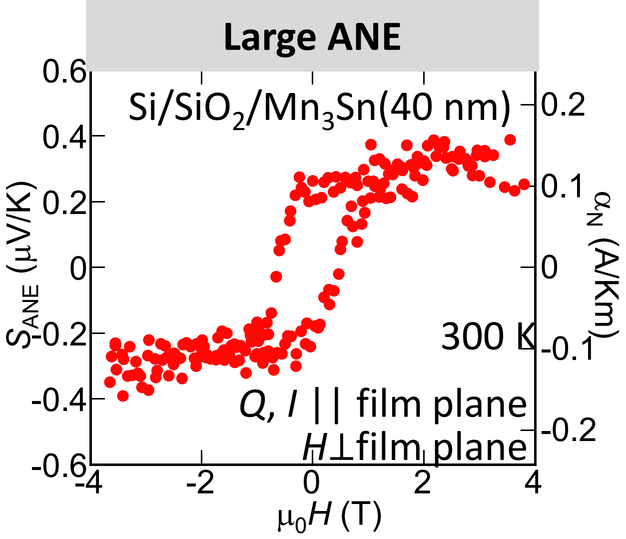

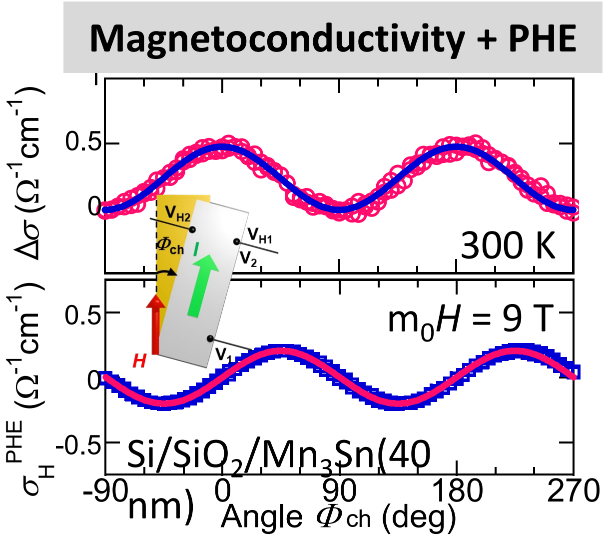

*Tsai⁺, Higo⁺ et al., Nature **580**, 608 (2020).*

■ Evidence for the presence of Weyl fermion

1. ARPES **difficult for polycrystalline thin films**
2. Large ANE beyond the empirical law with *M*
   100-1000 times larger ANE than that expected from *M*
3. Chiral anomaly through the MC and PHE
   MC : $\sigma = \sigma_{\perp} + \Delta\sigma_{chiral}\cos^2\Phi_{ch}$, PHE : $\sigma^{PHE}_{H} = \Delta\sigma_{chiral}\sin\Phi_{ch}\cos\Phi_{ch}$

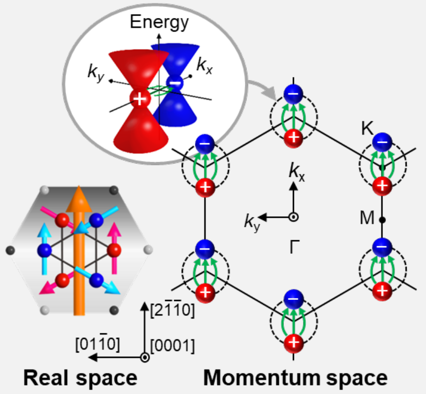

Nandy et al., PRL 119, 176804 (2017).

Angular dependence of MC & PHE is well fitted by the equations

Similar to the bulk, Mn_3Sn films should have a Weyl semimetal state

Electrical Switching in Mn_3Sn/metal devices

*Tsai+, Higo+ et al., Nature **580**, 608 (2020).*

Experimental setup

Si/SiO_2/Ru(2)/**Mn_3Sn(40)/Pt or W or Cu**/AlO_x(5)

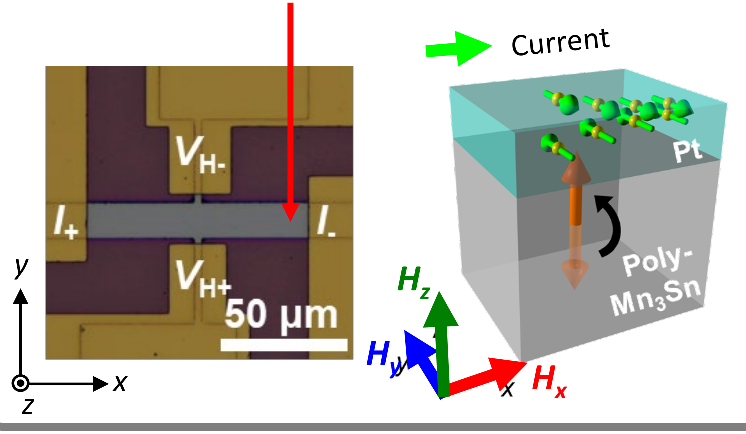

Hall bar device

W/L=16 μm /96 μm

Read & Write Current

I (read) = 0.2 mA

$|I$ (write)$|$ < 80 mA

@ R.T.

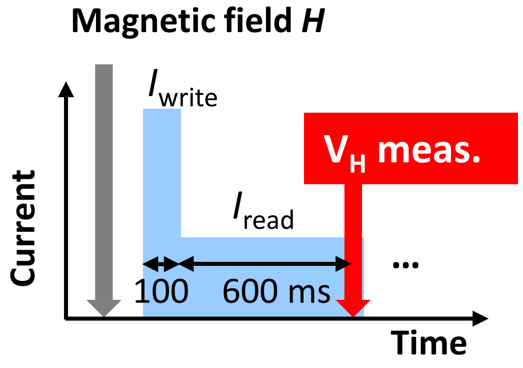

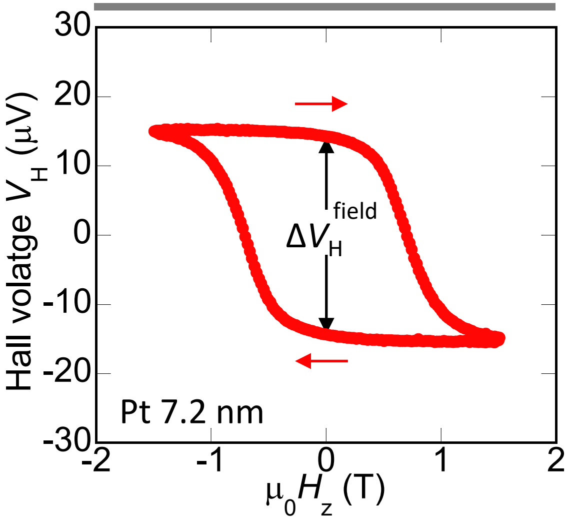

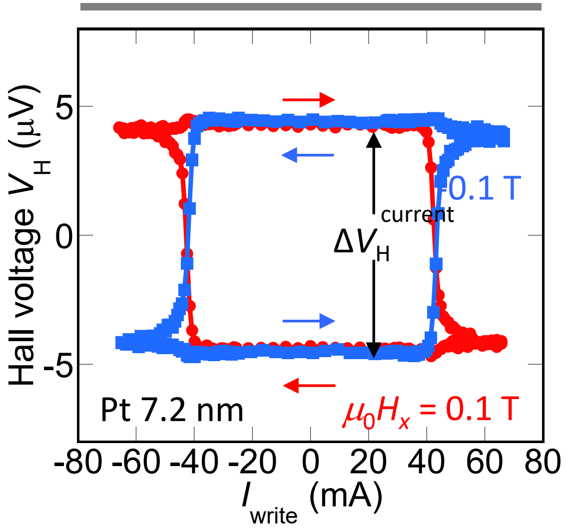

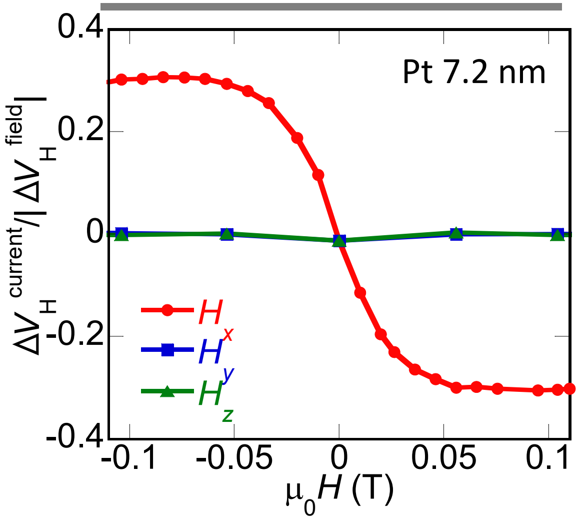

Symmetry consistent with SOT switching of the perpendicular *M*

SOT switching in Mn_3Sn/metal devices

Tsai+, Higo+ et al., Nature ***580****, 608 (2020).*

Pt: θ_{SH} >0 | **Cu: θ_{SH} ~ 0** | **W: θ_{SH} < 0**

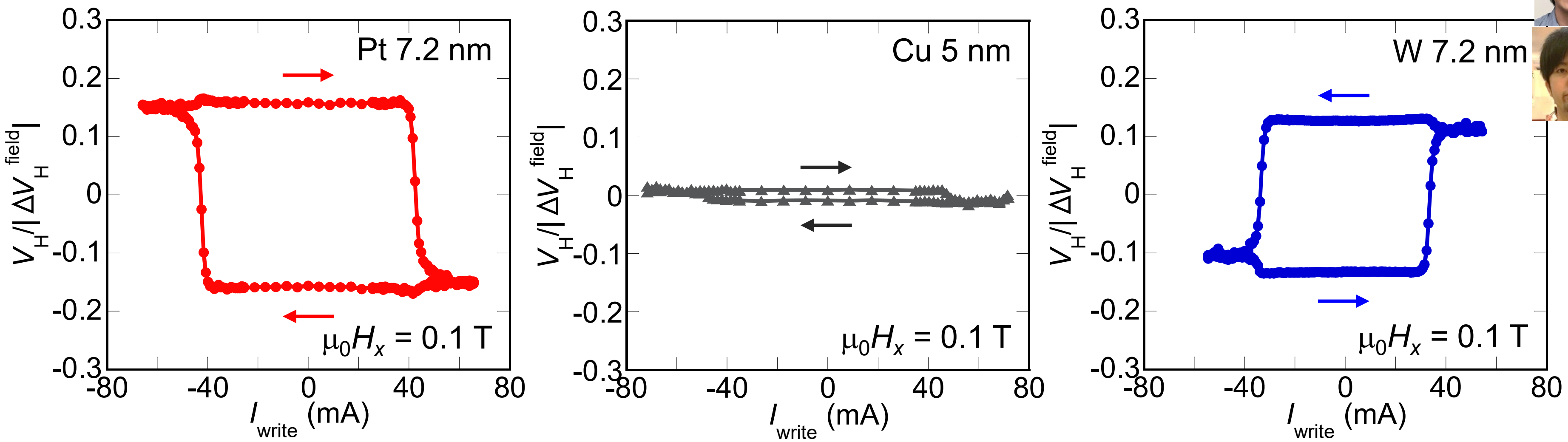

■ The sign of the spin Hall angle θ_{SH} determines the sign of V_H

➡ **SOT from SHE in heavy metal (HM) layer** ~~Oersted field~~

■ Critical current density : 2×10^{11} A/m^2 in Pt, 5×10^{10} A/m^2 in W

Comparable to other systems 【FM】~10^{12} A/m^2, Miron *et al.*, Nature (2011); Liu et al., Science (2012).
【AFM/FM】10^{10} A/m^2, Fukami *et al.*, Nat. Mater. (2016).
【Collinear AFM】10^{10} A/m^2, Wadley *et al.*, Science (2016).

The same switching protocol as that used for the FM/HM devices

Article

Perpendicular full switching of chiral antiferromagnetic order by current

https://doi.org/10.1038/s41586-022-04864-1

Received: 15 November 2021

Accepted: 12 May 2022

Tomoya Higo[1,2,9], Kouta Kondou[2,3,9], Takuya Nomoto[4,5], Masanobu Shiga[6], Shoya Sakamoto
Xianzhe Chen[6], Daisuke Nishio-Hamane[6], Ryotaro Arita[2,3,4], Yoshichika Otani[2,3,6,7],
Shinji Miwa[2,6,7] & Satoru Nakatsuji[1,2,6,7,8] ✉

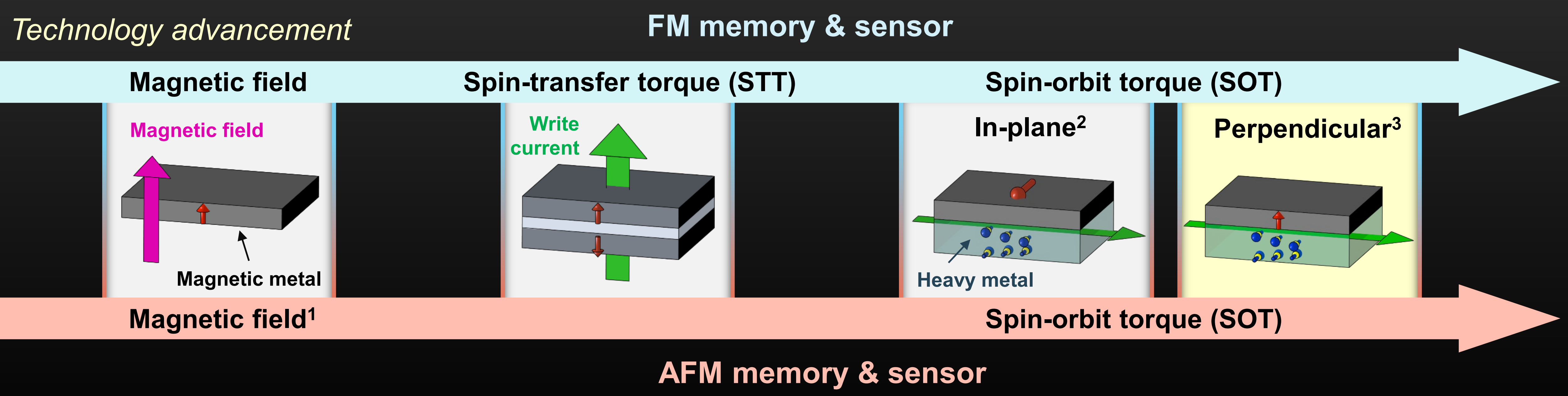

[1] S.N., Kiyohara, & Higo, Nature (2015). [2] Wadley et al., Science (2016); Moriyama et al., Sci. Rep. (2018); Chen et al., PRL (2018). [3] Tsai$^+$, Higo$^+$ et al., Nature (2020).

Mn_3Sn multilayer : fabrication & characterization

MBE

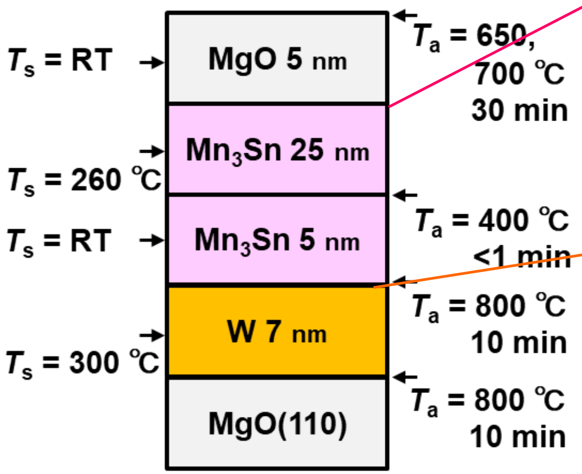

RHEED

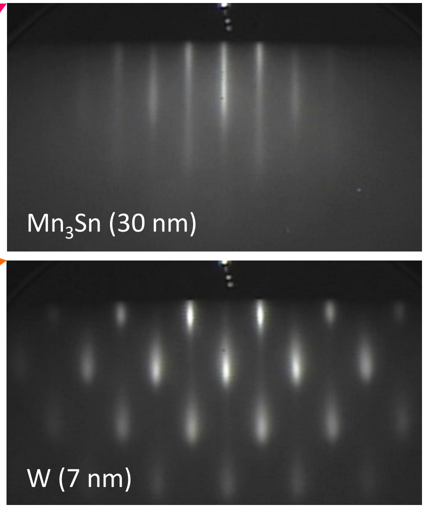

TEM

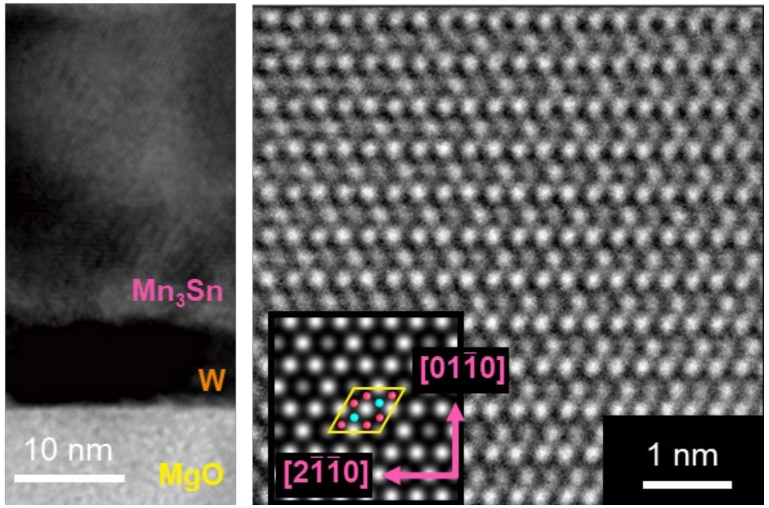

XRD

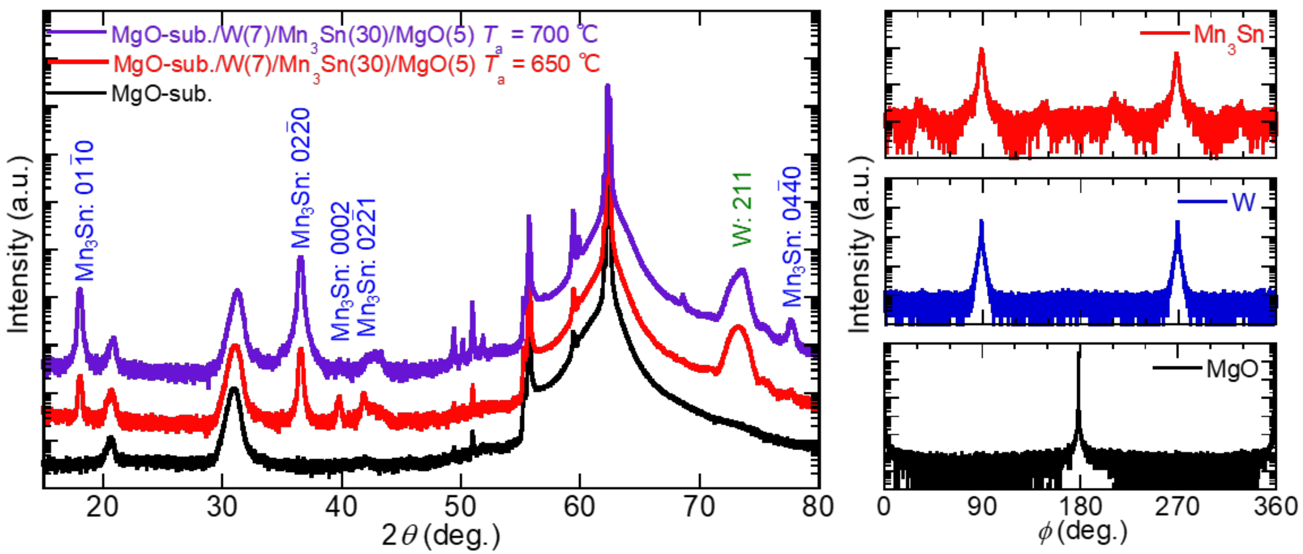

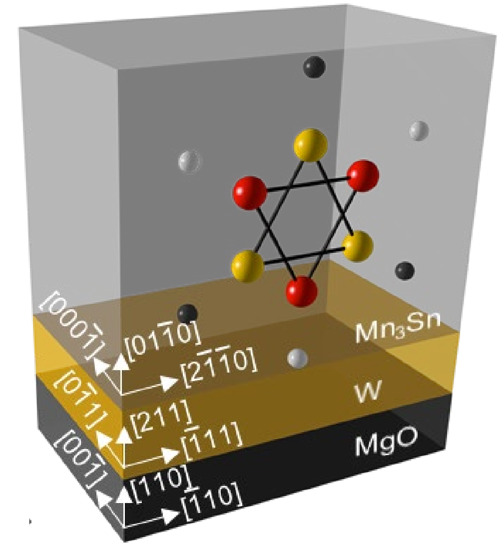

(01̄10)-oriented epitaxial Mn_3Sn layer was obtained by MBE

Strained Epitaxial Mn_3Sn layer

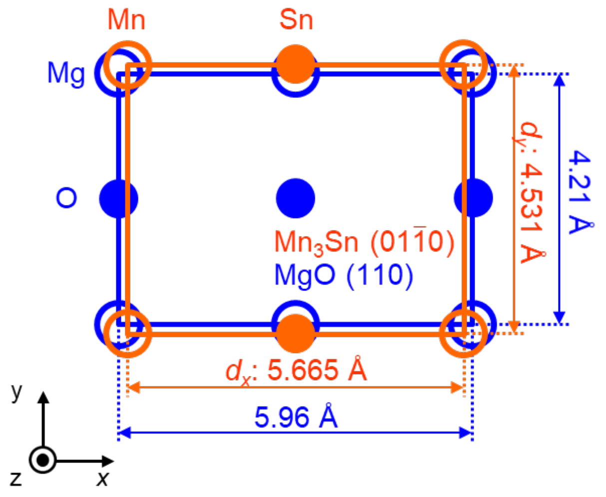

XRD

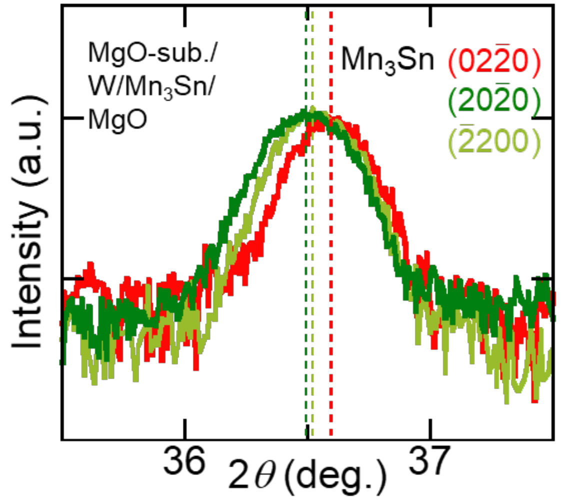

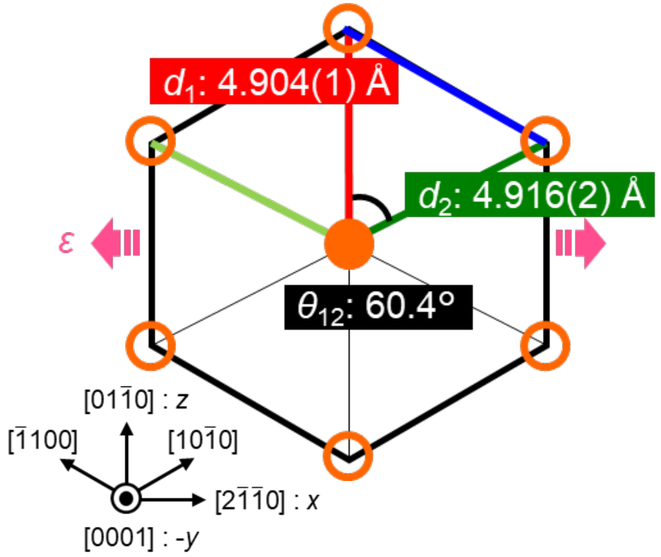

- **In-plane tensile strain ~0.2 % || [2$\bar{1}\bar{1}$0] in Mn_3Sn due to lattice mismatch between Mn_3Sn & MgO**

Mn_3Sn : d_x = 5.665 Å & d_y = 4.531 Å in (01$\bar{1}$0)
MgO : d_x = 5.96 Å & d_y = 4.21 Å in (110)

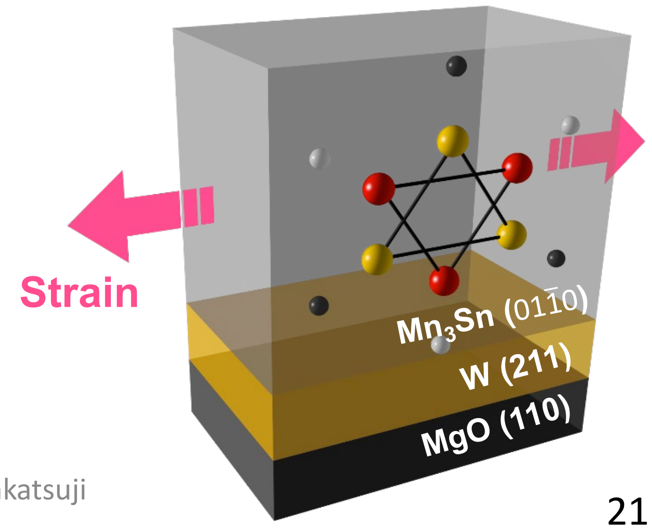

MBE-grown (W/)Mn_3Sn layer : transport properties

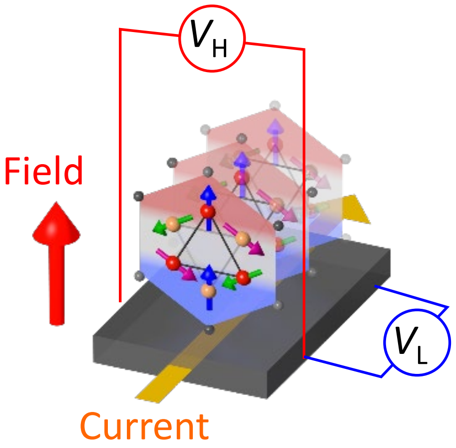

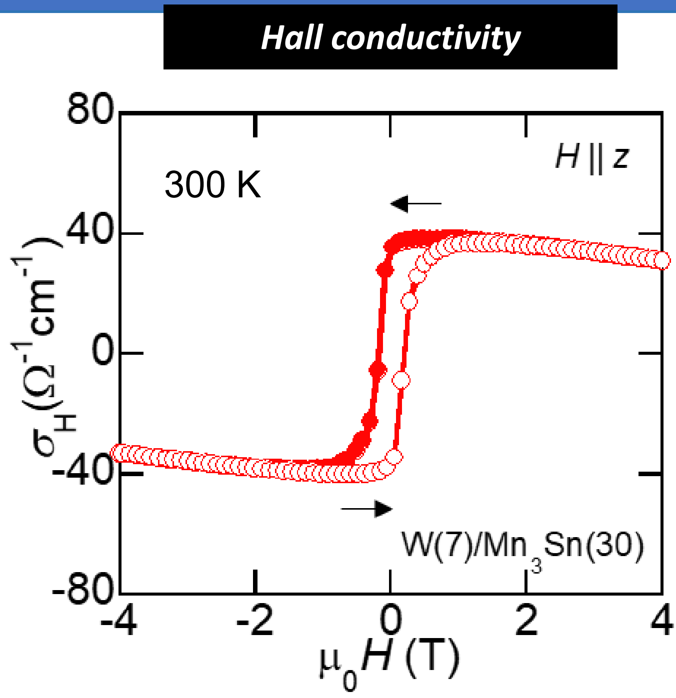

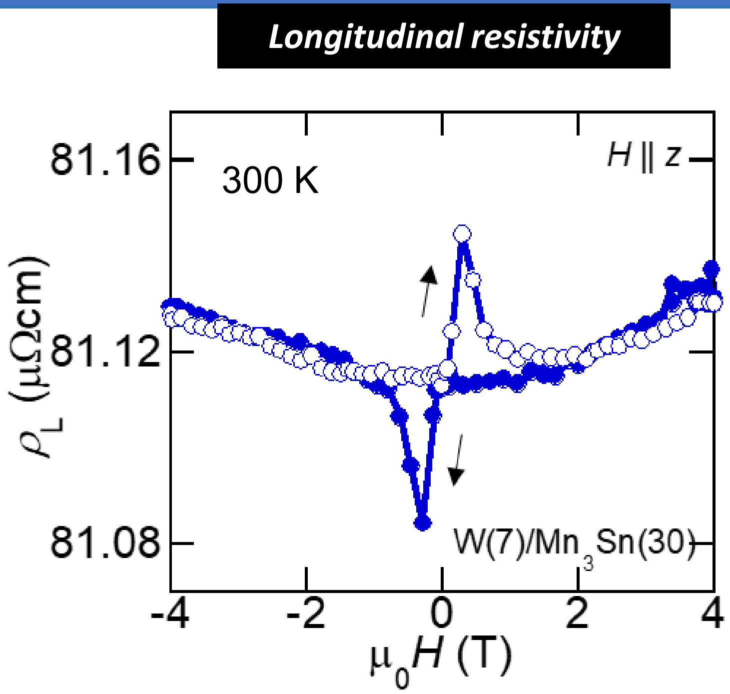

- Large AHE $\boldsymbol{\sigma_H}$ **~ 40 Ω^{-1}cm^{-1}** (Bulk : 30-40 Ω^{-1}cm^{-1}, Film : 20-30 Ω^{-1}cm^{-1})
- Small coercivity **$\mu_0 H$ ~ 0.15 T** (Bulk : 0.05 T, Film : 0.6 T)
- Asymmetric magnetoresistance ⇒ large magnetic domain

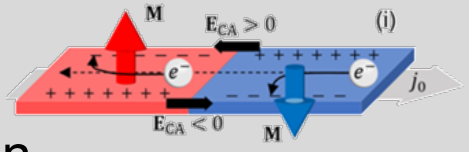

Sugimoto et al., Commun. Phys. ***3****, 111 (2020).*

High crystallinity MBE-grown Mn_3Sn layer is achieved !

First demonstration of full electrical switching in an antiferromagnet

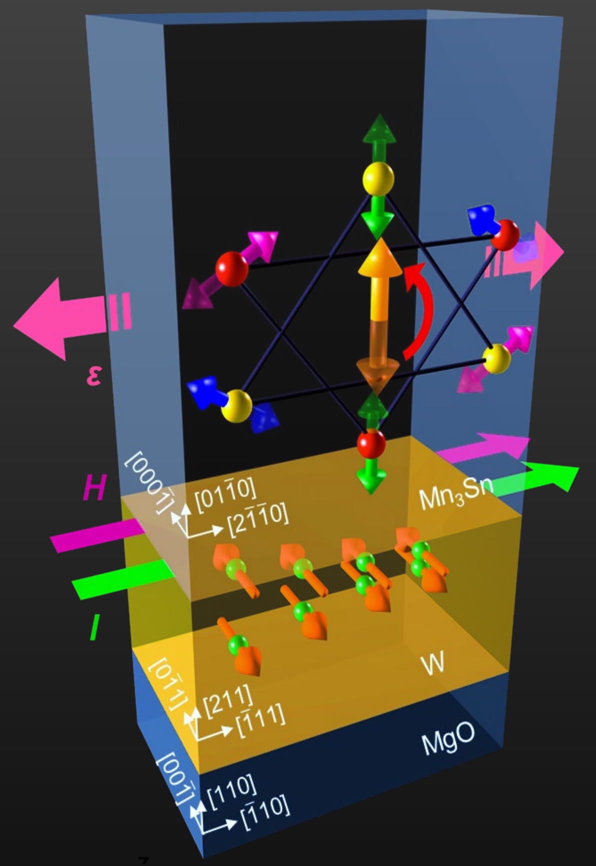

- Heavy metal (HM)/Mn_3Sn heterostructures fabricated by molecular beam epitaxy (MBE)
- Epitaxial in-plane tensile strain

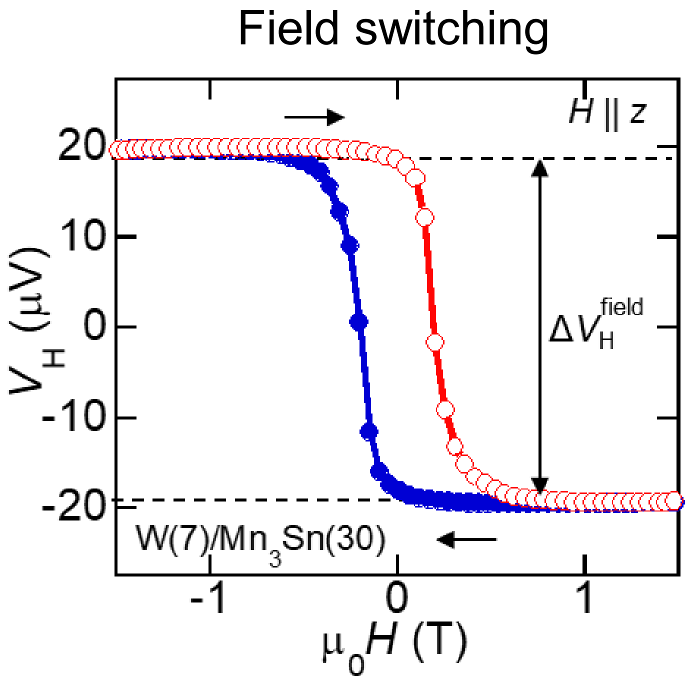

The first demonstration of 100 % electrical switching in an AFM material!
→ Crucial for high-speed operation and dense integration.

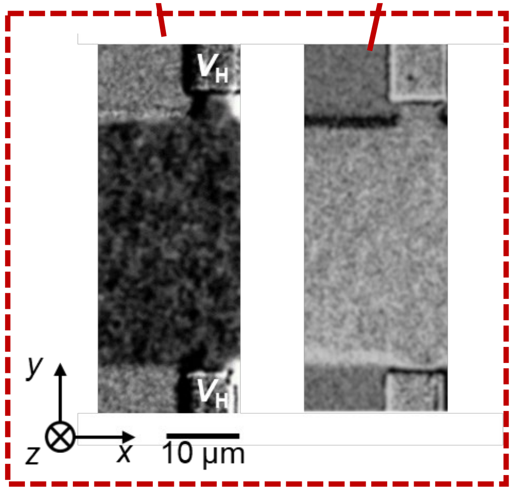

full switching confirmed by polar MOKE

Higo*, Kondou* *et al.*, Nature (2022).

Mechanism of current induced switching

In-plane tensile strain stabilizes perpendicular magnetic anisotropy through piezomagnetic effect.

Spin current through SHE apply spin torque constructively to each sublattice.

Perpendicular magnetic anisotropy (PMA)

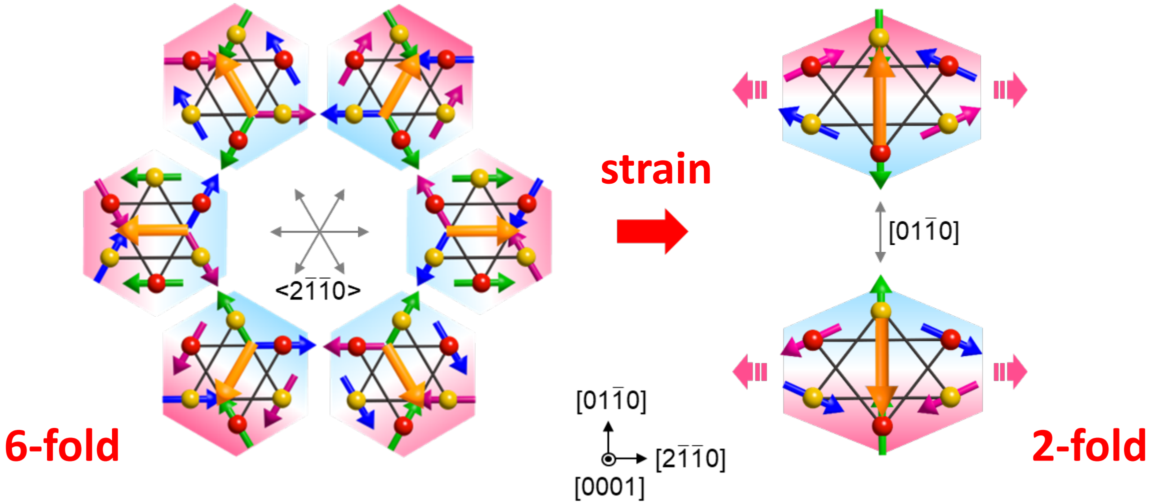

Current induced perpendicular switching

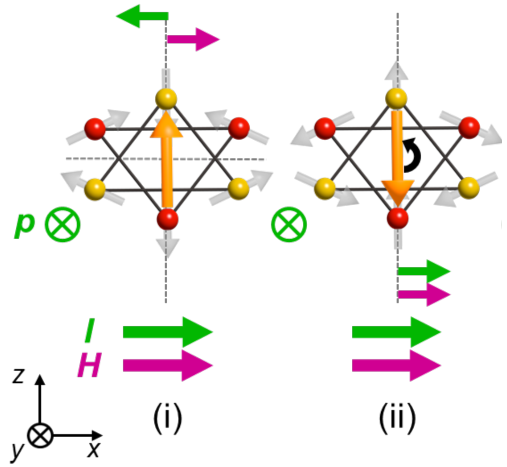

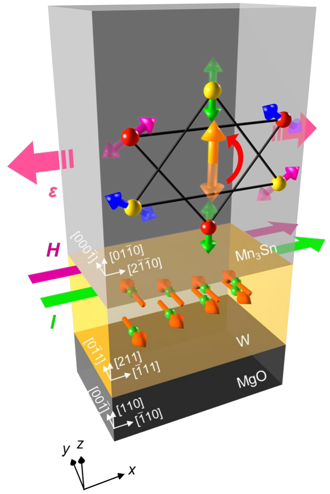

In-plane tensile strain can induce the perpendicular switching

Mechanism of current induced switching

In-plane tensile strain stabilizes perpendicular magnetic anisotropy through piezomagnetic effect.

Spin current through SHE apply spin torque constructively to each sublattice.

Change in current/field direction sets switching deterministically.

Efficient switching without intermediate state.

Numerical simulations

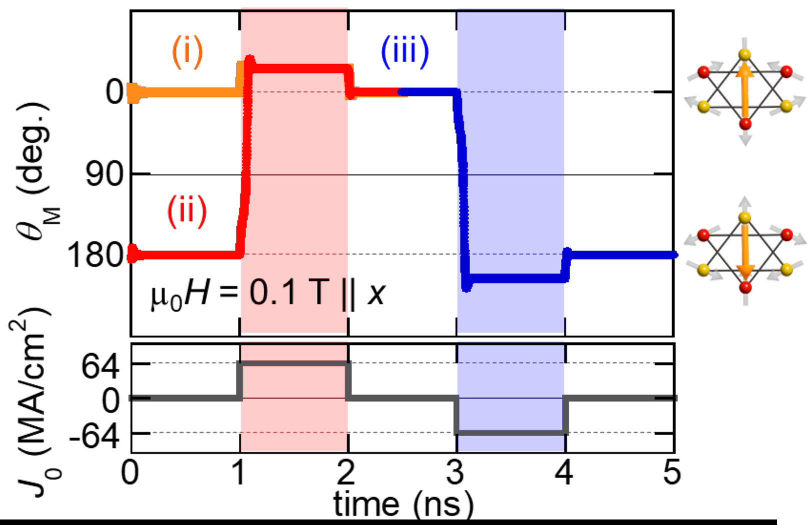

Current induced perpendicular switching

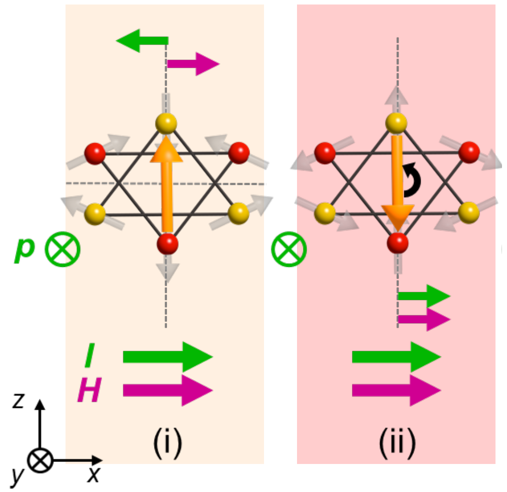

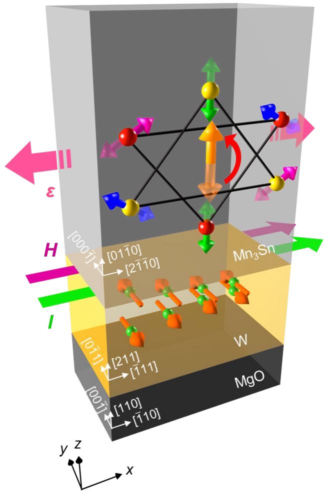

In-plane tensile strain can induce the perpendicular switching

$J_{write}^{W,theory}$ ~ 50 MA/cm^2 consistent with our observations

Summary

- Giant Transverse Responses in Topological Magnetic Semimetals beyond the magnetization scaling.

- First Strain Control of Sign of AHE in Antiferromagnet by Large Piezomagnetism of Mn3Sn

- First Full Electrical Control and Readout of AF Weyl semimetallic state

  Writing: Four Terminal SOT Switching of AF State

  Reading: AFM Tunneling Magnetoresistance